Study on outdoor environmental temperature on fire-induced smoke characteristics with hybrid exhaustion in atrium-type subway station

Desheng Xu [a], Yanfeng Li [a*], Tianmei Du [a], Hua Zhong [b*], Junmei Li [a], Jiaxin Li [a], Youbo Huang [c]

a *Beijing Key Laboratory of Green Built Environment and Energy Efficient Technology, Beijing University of Technology, Beijing, China*

b *School of Architecture, Design and Built Environment, Nottingham Trent University, Nottingham NG1 4FQ, United Kingdom*

c *College of Safety Engineering, Chongqing University of Science and Technology, Chongqing, China*

Abstract

This paper investigates the influence of outdoor ambient parameters on fire-induced smoke characteristics inside the station under hybrid exhaustion. Full-scale experiments were conducted both in summer and winter under different fire scenarios. And a series of numerical simulation works were carried out to study the effect of significant outdoor ambient parameters based on the results of orthogonal experimental design method. Temperature profile above the fire, smoke movement inside the station and smoke extraction efficiency were systematically analysed. Results show that the outdoor temperature changes have a larger influence on atrium fires than on concourse and platform fires. And the effect of the outdoor air temperature on fire-induced smoke movement could be divided into two regions according to the criteria value of Ar. It was found the cold outside air (Ar < 1) in winter would enter the station through the natural openings at the top of the atrium, inhibiting the smoke diffusion vertically and contributing to horizontal propagation. With the outdoor temperature and fire heat release rate increases, the smoke extraction efficiency shows a growth trend. Besides, empirical models were established to estimate the vertical temperature profile inside the atrium station taking the effect of outdoor temperature into consideration. And the predicted values by the proposed model are in good agreement with the full-scale experimental data. This work could technically support the smoke prevention design and fire emergency in practical metro station projects.

Keywords: Full-scale experiments; Fire-induced smoke; Temperature profile; Smoke extraction efficiency; Atrium-type metro station.

---

[*] postal address: Beijing University of Technology, Beijing 100124, China
E-mail address: liyanfeng@bjut.edu.cn, 2848765191@qq.com
E-mail address: hua.zhong@ntu.ac.uk

Nomenclature		T_s	smoke temperature (°C)
Ar	Archimedes number	T_{in}	air temperature inside the station (°C)
c_p	The specific heat capacity of air (kJ/kg·K)	T_{out}	air temperature outside the station (°C)
$CO_{natural}$	CO concentration exhausted from the roof openings (ppm)	t	burning time (s)
		V	volume of airflow (m³)
CO_{total}	CO concentration produced by the fire (ppm)	v_s	velocity of the smoke plume in the vertical direction (m/s)
$D*$	characteristic diameter of grid size	v_x	outdoor air velocity in X direction (m/s)
f	thermal buoyancy momentum (kg/s·m²)	v_z	outdoor air velocity in Z direction (m/s)
f_b	buoyancy momentum (kg/s·m²)	z	smoke vertical height (m)
f_g	gravitational force (kg/s·m²)	ΔT_{max}	maximum smoke temperature rise (K)
H	atrium height (m)	ΔT	smoke temperature rise (K)
h_s	smoke layer height (m)	*Greek letters*	
h_{sm}	maximum smoke layer height (m)	ρ_s	smoke density (kg/m³)
HRR	heat release rate (kW)	ρ_{in}	density of ambient air inside the station (kg/m³)
$m_{natural}$	smoke exhausted from the roof openings (kg/s)	ρ_{out}	density of ambient air outside the station (kg/m³)
m_{total}	smoke produced by the fire (kg/s)	η	smoke exhaustion efficiency through natural exhaustion
OED	orthogonal experimental design	*Subscripts and subscripts*	
Pr	Prandtl number	*	dimensionless expression
Q	heat release rate (kW)	in	inside the station
Q_c	convective heat release rate (kW)	out	outside the station
Sc	Schmidt number	s	smoke

1

1

1.Introduction

As a key part of the passenger transport network in the city, metro station serves as a crucial hub for connecting different metro lines. The outstanding advantages, such as convenience, efficiency and safety, can effectively ease the strain caused by large passenger volume in urban surface traffic (Domingo et al., 2011; Hu et al., 2020; Izadi et al., 2021). The establishment of the metro station has ushered in a highly rapid growth recent years (Lin et al., 2021; Dong et al., 2023). By the end of 2022, the number of cities with metro station in China has reached 55, with a total of 8,008 kilometers in operation for urban rail transport (China Urban Railway Transit Association, 2023). Due to the constrained environment and few exits of underground space, toxic smoke would threaten the personnel safety under fire scenarios, causing great loss of life and property (Hu et al., 2014; Giachetti et al., 2016; He et al., 2023). Particularly, fire accidents are more likely to occur in metro stations with complex structures and high pedestrian traffic (Lan et al., 2022; Long et al., 2023). For instance, typical subway fire events in Daegu, Baku and London were disastrously happened, leading to a large number of casualties (Jang et al., 2022). While many factors affect the fire development and smoke movement in a metro station, such as the ventilation pattern, construction dimension, fire location and environmental conditions. (Luo et al., 2014; Chen et al., 2022). Therefore, the key influences of fire-induced smoke in the station needs to be explored in detail.

According to Chinese standard for metro design (GB 51251, 2017) and related design documents (China Railway First Survey and Design Institute Group Co and LTD, 2013; Urban Construction Design & development Group Co and LTD, 2015), the ventilation patterns in platform and concourse should be jointly activated to exhaust smoke from the subway station. And the smoke prevention systems in standard stations are normally comprised of air supply system and smoke exhaust system in concourse and platform, as well as track exhaust fan system (TEF) and tunnel ventilation fan system (TVF). Hybrid smoke exhaust pattern is commonly used in the actual operated metro station, which is a combination of mechanical ventilation and natural ventilation. In addition, the Platform Screen Door (PSD) system is the key facility to controlling the fire smoke between the platform and tunnel, and the effect of PSD type and platform ventilation mode on smoke diffusion was researched (Roh et al., 2009; Meng et al., 2014; Wang et al., 2018; Li et al., 2021a). As for the new metro stations currently being built, most of them are full-height screen doors. The screen doors are all closed during the trains service and are only opened when people are loading the trains. Therefore, the screen doors are only considered to open under train fire scenarios and stopped at the platform. For fire scenarios in station space, such as baggage fires and small equipment fires, the screen doors are constantly closed.

Full-scale tests are able to directly and fairly accurately produce results that are similar to the actual fires (Johansson et al., 2015; Melcher et al., 2016; Tian et al., 2017). A series of difficult full-scale fire experiments were carried out by some scholars and valuable research findings of smoke characteristics

3

under fire scenario in metro station were obtained. Based on full-scale fire experiments (Long et al., 2020), the smoke movement under different fire source locations on the platform and concourse of a double-theory island station were investigated. It was found that the variation in ventilation pattern has a more noticeable effect on smoke layer height and temperature distribution in the near-fire area. A series of fire experiments were carried out at an interchange metro station (Liu et al., 2020). Results showed that the combined action of the mechanical smoke extraction system and the air supply system provides effective control of the smoke diffusion from the platform. And maintaining a downward airflow at the stairway between the station concourse and platform is essential to prevent the smoke spreading. Xu et al., (2021) conducted field fire experiments in three metro stations with different platform heights. By analysing the temperature distribution as well as the smoke spread, a correlation formula between the optimum smoke extraction velocity and the station platform height was established. Liu et al., (2022) conducted full-scale fire tests in subway platform to study the effective measures to prevent the smoke propagation. It could be found that the increasing the depth of the smoke curtain could reduce the amount of smoke extraction to some extent. And a prediction model for determining the minimum smoke curtain depth was proposed. Seven full-scale hot smoke tests were carried out in a subway station without ventilation systems (Cheng et al., 2023). Based on the temperature distribution and smoke diffusion, the fire regions were divided into fire plume zone and ceiling jet zone. It was discovered that the increase of heat release rate would enhance fire plume entrainment and reduce the airflow stability. Full-scale fire tests were carried out in a long-large subway tunnel with mechanical exhaust systems to study the ceiling smoke temperature. From the experimental results, the smoke movement space was divided into three regions and the temperature decay prediction models were proposed.

Since full-scale experiment is more difficult and expensive to be conducted, numerous researches about smoke characteristics (Liu et al., 2019; Li et al., 2021b) and prevention (Zhao et al., 2016; Long et al., 2021) for metro station fires have been carried out through model-scale experiments (Ji et al., 2011; Meng et al., 2017) and numerical simulation (Rie et al., 2006; Zhou et al., 2018). In terms of ventilation modes design, Gao et al., (2012a; 2012b) pointed out that the hybrid ventilation system could inhibit the smoke propagation more effectively than conventional mechanical ventilation by simulation method. Luo et al., (2014) studied the smoke extraction efficiency with different ventilation systems and vent layouts in a three-theories interchange station. It could be found that the optimal smoke extraction effect is guaranteed with the condition of air supplied in the first basement, smoke exhausted in the second basement and not ventilated in the third basement. Gao et al., (2015) revealed the influence of a dome on the movement of fire-induced smoke in an atrium-type subway station, and it was found the increasing volume of the dome can enhance the storage of fire smoke and reduce the smoke concentration within the station. Wang et al., (2019) carried out reduced-scale experiments and numerical simulation to study smoke movement and smoke layer stability under hybrid ventilation mode. And the critical value of ventilation coefficient was proposed to provide low ceiling temperature and improved smoke layer stability. Liu et al., (2021) numerically researched the minimum airflow velocity at the stairways for

preventing smoke propagating from the platform to the upper floor in case of a platform fire. And it was found that the setting of side slabs at stairways is an effective measure to lower down the required exhaust capacity. Six air control strategies were developed for smoke dispersion by varying the air supply and exhaust outlets of each floor in a cross-interchange subway station (Wang et al., 2022). And an intelligent decision-making method of disaster rescue was proposed based on the smoke control modes. Chen et al., (2022) focused on the smoke extraction efficiency of different vent layouts, and found that the lateral ventilation pattern could significantly depress the toxic smoke density and improve the visibility in the subway station. Long et al., (2023) combined numerical simulations and model-scale experiments on a double-island metro station to investigate the smoke control methods under different fire scenarios and various ventilation modes.

In recent years, a large number of metro stations with tall atrium have been built for the convenience of pedestrians and requirements of illumination. The connection of the upper concourse and lower platform makes it more difficult to prevent smoke diffusion in case of fire. Several scholars studied the smoke spread and temperature distribution in atrium-type metro stations (Chow et al.,1995; Gao et al., 2015; Ivanov et al., 2021). However, almost researches are focus on the ventilation strategies and smoke prevention facilities for subway fires. Few studies have addressed the effect of outdoor environment conditions on fire smoke extraction in atrium-type metro stations. The atrium roof window is exposed to solar radiation and outdoor air, which can affect the airflow movements through the openings (Cheng et al., 2020). According to the SFPE handbook of fire protection engineering (Beyler et al.,1995), the temperature difference between indoor and outdoor air has a significant influence on the movement of fire-induced smoke. For example, the thermal barrier effect would occur in the hot summer months, restricting the smoke rises in the vertical direction. Therefore, the influence of outdoor environmental parameters on smoke characteristics should not be neglected and need to be revealed for smoke control under different fire scenarios in the atrium-type metro station.

The aim of this work is to expose the mechanics of the influence of outdoor ambient parameters on airflow through the atrium roof openings and smoke movement inside the station. Full-scale experiments were conducted at an atrium-type metro station in Beijing, China, both in summer and winter under different fire scenarios. Based on the results of orthogonal experimental design table, the significant outdoor ambient parameters were determined and a series of numerical simulation works were carried out. Temperature profile, smoke diffusion and smoke extraction efficiency were analysed. According to the criteria value of Ar, the effect of the outdoor air temperature on the smoke movement is divided into two regions. And the prediction model of vertical temperature profile was proposed. Results also show that the cold outdoor air temperature would create an obstacle to the upward movement of the smoke at the initial fire stage, reducing the efficiency of smoke extraction. This work could technically support the smoke prevention design and fire emergency in practical subway projects with tall atrium.

2.Therotical Analysis

Once a fire occurs at the atrium space, smoke could rise vertically by thermal buoyancy effect. It is mostly produced by the pressure difference between the high temperature smoke and inside air (Ji et al., 2013):

$$f = (\rho_{in} - \rho_s)gh_s \tag{1}$$

where f is the thermal buoyancy momentum; ρ_{in} is the density of ambient air inside the station; ρ_s is the density of smoke; g is the gravity acceleration and h_s is the smoke layer height.

As the smoke gradually rises in the vertical direction, the height of the smoke layer h_s increases. Additionally, the surrounding entrainment air would continuously integrate into the hot smoke, causing the temperature to decay and t_s to decrease (Tan et al., 2021). In this procession, the relationship between buoyancy forces and the inertia forces could be approximately expressed as (Liu et al., 2021):

$$(\rho_{in} - \rho_s)gh_s = \frac{1}{2}\rho_s v_s^2 \tag{2}$$

where the v_s is the velocity of the smoke plume in the vertical direction, and it can be written in the following:

$$v_s = \sqrt{2\frac{\rho_{in} - \rho_s}{\rho_s}gh_s} \tag{3}$$

The parameters of the outside environment have strong influences on the movement of fire smoke, e.g. fire scenarios in underground stations (Xu et al., 2021), road tunnels (Fan et al., 2017) and high-rise buildings (Qi et al., 2014; Bilyaz et al., 2021). Especially in the atrium with a in tall space, the stack effect by the fire plume would increase significantly. During the hot summer days, the roof window is exposed to solar radiation and high temperature of the outdoor air. It causes the temperature of the roof air gradually rises, eventually forming a layer of hot air thickness under the roof and creating a temperature gradient field inside the station with rising temperatures from the bottom to the top (Filis et al., 2021). As the fire smoke propagate vertically under the thermal buoyancy, temperature gradually decreases, and the hot air layer on the roof would become a barrier to the smoke exhausting from the roof openings (Xie et al., 2023). This phenomenon is known as the "thermal barrier effect". In this condition, the maximum smoke height that a fire-generated plume in a tall space could be expressed as (Beyler et al., 1995):

$$h_{sm} = 3.79\sqrt{\frac{T_{in}}{g(\rho c_p)^2}}^{1/8} Q_c^{1/4}\left(\frac{dT}{dz}\right)^{-3/8} \tag{4}$$

where h_{sm} is the maximum smoke layer height; Q_c is the convective heat release rate, which is assumed

1 to be 70% of the total heat release rate; $\frac{dT}{dz}$ is the ambient air temperature gradient in the vertical direction.

2   While in cold winter days, the temperature of the roof air is commonly below 0 ℃. And the inside

3 temperature T_{in} is higher than outdoor air temperature T_{out}. The pressure difference $\rho_{in} < \rho_{out}$ results in

4 the airflow from outside to the internal (Qin et al., 2009). It causes the outside air would enter the station

5 through the top roof openings, as shown in Fig. 1a. This phenomenon is called as the "reverse stack

6 effect". As the smoke reaches the top ceiling openings, the pressure difference between the outdoor air

7 and smoke could cause a buoyancy momentum f_b. While the for the airflow at the roof window, it is also

8 subject to the gravitational force f_g of the outside air above. These two forces act in opposite directions,

9 as shown in Fig. 1b. The A_r number was used to quantify the ratio of thermal buoyancy to gravity

10 (Yamasawa et al., 2021):

$$Ar = \frac{f_b}{f_g} = \frac{(\rho_s - \rho_{out})Vg}{\rho_{out}V} = \frac{(\rho_s - \rho_{out})}{\rho_{out}} g \qquad (5)$$

12   Assuming that the pressure of the plume and the ambient air are the same, according to the equation

13 of state for an ideal gas:

$$\frac{\rho_s - \rho_{out}}{\rho_{out}} = \frac{T_{out} - T_s}{273 + T_{out}} \qquad (6)$$

15   Thus, the Eq. 4 can be rewritten as:

$$Ar = \frac{T_{out} - T_s}{273 + T_{out}} g = \frac{\Delta T_{os}}{273 + T_{out}} g \qquad (7)$$

17 where ΔT_{os} is the temperature difference between smoke at the roof window and outside air. If $A_r > 1$,

18 the upward thermal buoyancy force f_b is greater than the downward gravitational force f_g and the smoke

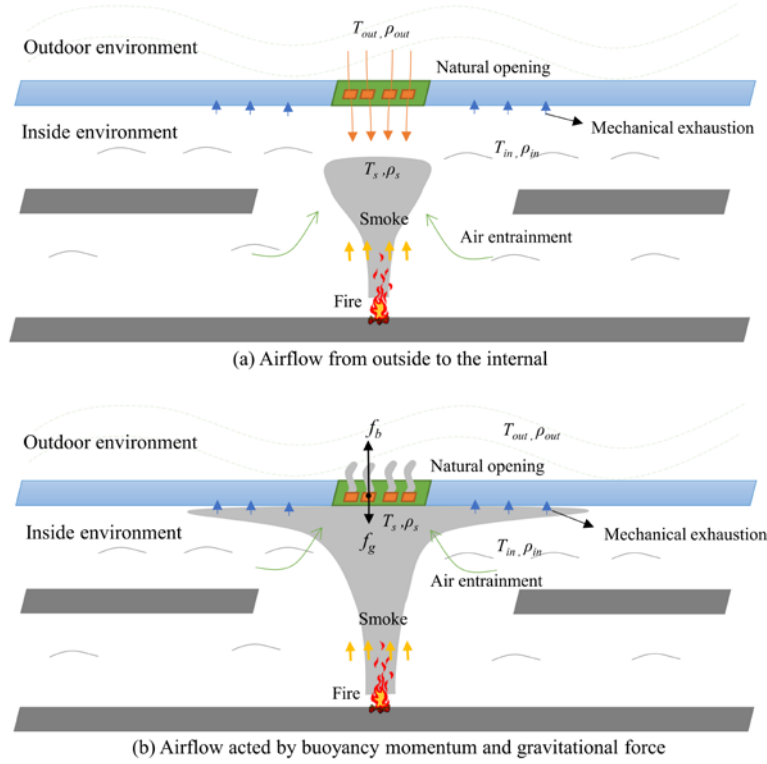19 would flow through the opening. Conversely $A_r < 1$, the smoke cannot escape from the opening.

(a) Airflow from outside to the internal

(b) Airflow acted by buoyancy momentum and gravitational force

1

2   Fig. 1. Diagram of smoke movement in atrium station fire by reverse stack effect

3 **3. Full-scale experiment setup**

4 **3.1 The experimental station**

5   A series of full-scale experiments were carried out in an atrium-type subway station, servicing the

6 subway line 6 at Beijing. The station is an underground double-storey island station, with the main

7 equipment with a partially open central slab in the public area and a connected atrium. As shown in Fig.

8 2, the net dimensions of the station hall concourse were 126 m(Length) × 27 m(Width) × 5.7 m(Height)

9 with a platform geometry of 153 m × 11 m × 4.7 m. The atrium is located in the middle of the public area

10 with a size of 58 m in length, 10 m in width and 11 m net height. The constructions and installations of

11 the subway station was already accomplished before fire experiments, such as the natural smoke vent at

12 the roof window and the mechanical ventilation system.
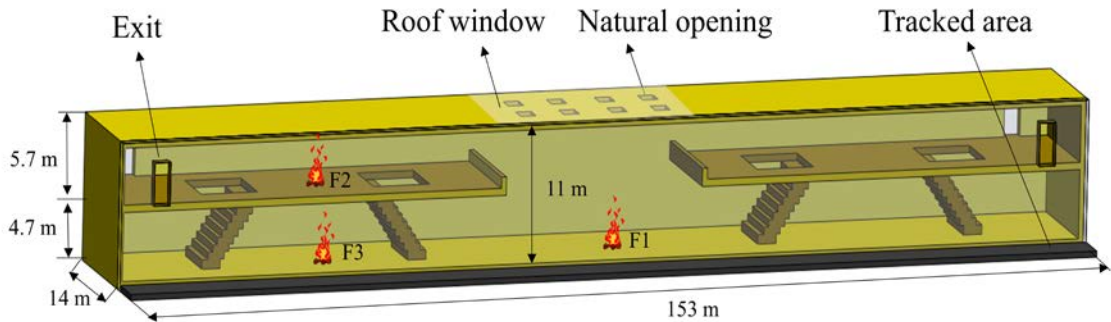

13

14   Fig. 2. Layout of the full-scale experimental subway station.

8

1   The distribution of exhaust vents and air supply vents is shown in Fig. 3. For atrium and concourse

2 fires, all smoke vents in the concourse were opened and the total volume of exhaust smoke was 75.0 m^3/s.

3 In the case of a platform fire, the smoke exhaust vents (onside near the fire) on the platform and rail roof

4 were opened. The sum of the smoke volume were 13.6 m^3/s and 42.0 m^3/s respectively. In addition, the

5 supply vents in the platform (onside near the fire) should turn on the inversion mode for smoke exhaust.

6 The black and blue squares in Fig. 3 represent the exhaust and supply vents, and the arrows indicate the

7 direction of the smoke. There are 48 exhaust vents in the concourse with a size of 0.5 m × 0.5 m and 16

8 air supply vents with 1.0 m × 1.0 m. The total number of exhaust vents and supply vents in the platform

9 are 56 and 16 respectively, with the same size in the concourse. The details of the ventilation plan under

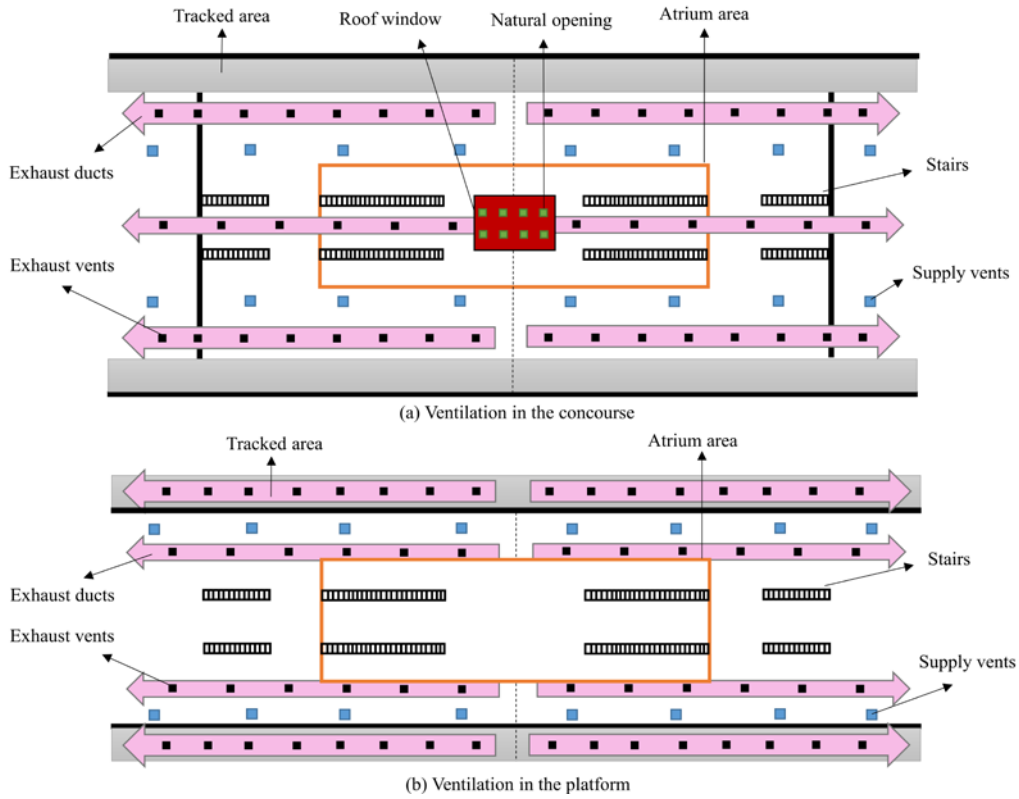10 fire scenario are listed in Table 1.

11

12   Fig. 3. Distribution of exhaust vents and air supply vents in the station.

13 **3.2 Fire source**

14   Luggage fires are considered to be the most common type of fire scenario in metro stations, and the

15 heat release rates are in the range of 0.7 — 2 MW (Long et al., 2020; Shi et al., 2021). In the full-scale

16 tests, ethanol (95%) and a smoke generator were employed as the fire source (Liu et al., 2020). The

17 smoke generator was consisting of smoke cake and pipe, and the ethanol (95%) was placed in a

18 combustion tray under the smoke generator, as shown in Fig. 4. The dimension of fuel pan internal the

19 combustion tray was about 0.5 m^2. Thus, the smoke plume was continuously heated to create a real fire

1   scene. Under the thermal buoyancy effect of the fire plume, the smoke produced by the fire source can

2   be well observed. In order to systematically investigate the effect of the outside environment on smoke

3   diffusion, the fire source was placed in three positions under the atrium, concourse and platform, as

4   shown in Fig. 2. And the total heat release rate of the fire source was set to 0.7 MW (Xu et al., 2021).

5   The full-scale tests were conducted both in summer and winter, the details of the test conditions are

6   shown in Table 1.

7   Table 1. Details about the full-scale test scenarios

| Scenario number	Fire source location	HRR (MW)	Smoke exhaust		Air supply		Inside temperature (°C)	Outside temperature (°C)	Outside Velocity (m/s)
			Concourse	Platform	Concourse	Platform			
No. 1	F1		Open	Closed	Closed	Open	15	8	0.8
No. 2	F1		Open	Closed	Closed	Open	18	20	0.3
No. 3	F2	0.7	Open	Closed	Closed	Open	15	8	0.8
No. 4	F2		Open	Closed	Closed	Open	18	20	0.3
No. 5	F3		Closed	Open	Closed	Inversion	15	8	0.8
No. 6	F3		Closed	Open	Closed	Inversion	18	20	0.3

8
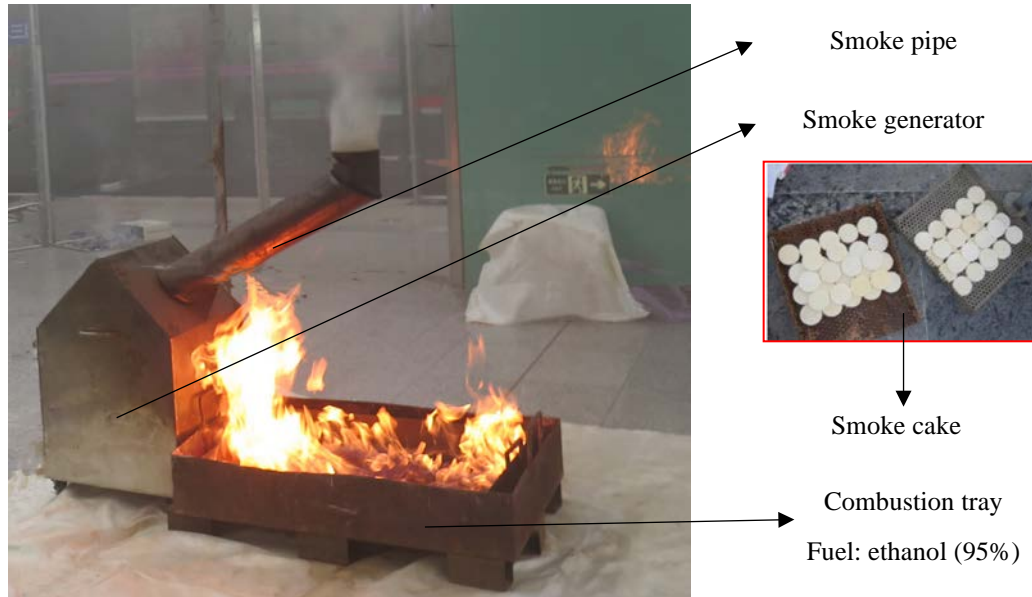
9   Fig. 4. Diagram of fire source in the full-scale test.

10   **3.3 Measurement system**

11   The measuring system was primarily composed of temperature sensors, acquisition device and

12   anemometer. A total of six measuring strings formed the temperature sensors in key areas of the metro

13   station. And the K-type thermocouples were used to record the temperature of measuring point, a range

14   of 0 — 1300℃ with accuracy of ± 0.75% (Xu et al., 2023). String #1 — String #4 were distributed 2.0

15   m around the fire source. And each measuring string was arranged with 7 thermocouples in a 1.5 m – 4.5

16   m altitude range. The thermocouple points on String #5 were set at 0.5 m interval directly above the fire

17   source to record the temperature decay. And the String #6 was vertically placed beneath the roof window

from 1.5 m to 11.0 m in the atrium area. The detail arrangements of measuring strings are shown in Fig.

5. All the temperature sensors were connected by acquisition devices of Agilent 34970A, and real time

data were recorded and stored. The outside environment of the subway station was measured by a TSI

high-precision miniature anemometer DP-CALC 8715 with an accuracy of ± 2%.

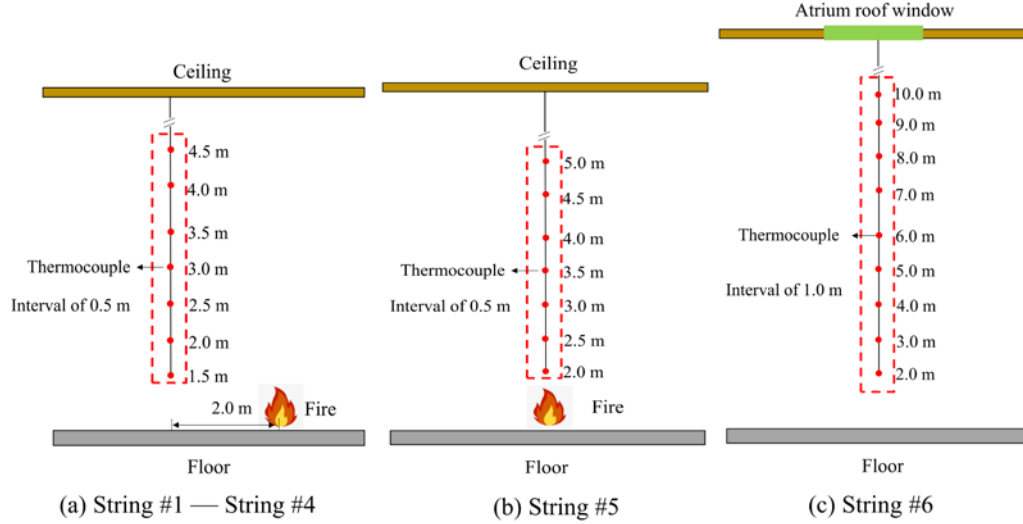Fig. 5. Diagram of thermocouple setting on each measuring string.

4. Numerical simulation settings

4.1 Physic model

In order to further study the influence of outside environment on smoke diffusion in subway station, a

series of numerical simulation woks were conducted. Fire scenarios was simulated by Fire Dynamics

Simulator (FDS) version 6.3.2, which has been developed by the US National Institute of Standards and

Technology (NIST) (McGrattan et al., 2018). The physical model was an atrium-type station with two

storey based on a 1:1 model of full-scale experiment. And the numerical model of the station is given in

Fig. 6. The dimensions of the platform are 158 m (Length)× 14 m(Width) × 5 m(Height), and the width

of the tracked is 4 m. And a full-screen door system is settled between the platform and tracked area. The

2nd floor is the concourse floor with the dimensions of 158 m × 14 m × 6 m. An atrium has been set up

in the public area with 50 m × 14 m × 11 m in size. There are four stairs connecting the platform and the

concourse floor in the metro station. And four exits in the concourse as the natural make-up air inlet.

Eight openings of the roof window are symmetrically arranged, with 2 m in length and 2 m in width.

According to Chinese standard GB51251 – 2017, the ventilation pattern needs to be a combination of

mechanical and natural ventilation in metro station containing an atrium space. Thus, the hybrid

ventilation pattern was employed in this paper (Peng et al., 2021) Once the fire occurs, both mechanical

and natural smoke extraction systems were used for fire ventilation. The openings of the roof window

were the natural smoke extraction outlets in the station. And the smoke exhaust vents were uniformly

1 distributed along the ceiling of the platform and concourse according to the experiments, with dimensions

2 of 0.5 m × 0.5 m. The fixed volume of exhaust smoke in the concourse was 75.0 m^3/s and the sum of the

3 smoke volume in the platform and railway was 42.0 m^3/s and 13.6 m^3/s, respectively. The platform screen

4 doors were supposed to be closed in case of the fire occurs in the station space (fire is located at A, B

5 and C). And once a fire breaks out on the metro train (fire is located at D), the platform screen doors

6 were opened to diffuse smoke. Fire source A was located in the central part of the station atrium. While

7 fire sources B and C were both on the centre line of the station along the Z axis, with X coordinates -47

8 m at concourse and platform, respectively. Fire source D was located in the railway tracked area, on the

9 centre line of the X axis. The dimensions of the fire source were all set 1.0 m× 1.0 m.

10 The HRR of fire source in full-scale experiments was only set as 0.7MW due to the safety of testers

11 and built subway station. The most common cause for subway station fire is luggage and suitcase carried

12 by passengers (Zhang et al., 2019), and the maximum HRR could reach 2 MW (Park et al., 2006; Zhang

13 et al., 2018). In the numerical simulations, the HRRs from 2 MW to 5 MW were considered as the most

14 unfavourable fire scene, which occurs at the atrium (fire is located at A). While for fire scenario at

15 concourse and platform (fire is located at B and C), the HRR was set as 2 MW. And a 5MW fire (Wang

16 et al., 2009; Gao et al., 2015) was set for the train fire (fire is located at D).

17 According to Chinese standard GB 50157-2013, the designed environment temperature inside the

18 station is around 20℃ over the year. While the air temperature of the outside environment changes with

19 the season. For example, the outdoor ambient temperature in Beijing can reach up to 40 ℃ in summer

20 and down to ‑ 20 ℃ in winter. It has a significant impact on the flow through the natural smoke vents

21 inside and outside the station. It should be stated that an extended area was created above the atrium with

22 a size of 50 m × 14 m × 7 m. Within this area, the environment parameters were changed by varying the

23 air supply velocity and temperature on two sides (v_x and v_z). In this way, the simulation of the outdoor

24 environment of a metro station is realized, and also allows for the outdoor parameter changes to have an

25 effect on the smoke movement under fire conditions inside the station.

26 **4.2 Boundary conditions setting**

27 The parameters of the construction boundary condition, such as the walls, ceilings, and floors of the

28 numerical model, were all set to be "INERT" with thermally thick concrete. The density was 2400 kg/m^3

29 and the conductivity was 2.0 W/(m·K) with the specific heat 0.9 kJ/(kg·K) (Predvoditelev et al., 1972).

30 The condition of "SPPULY" contained the supply vents on the ceiling and two sides of the extended area.

31 And a fixed air velocity was adopted in the supply vents. The station exits and the openings above the

32 atrium were set as "OPEN". The exhaust vents were set to be "EXHAUST" with the velocity of 2 m/s.

33 The T-square rapid fire was considered as the characteristic of the "FIRE", and the growth rate α was

34 adopted as 0.04689 kW/s^2 (Zhang et al., 2019; Hu et al., 2014). Eq. (8) presents the calculation formula

35 between heat release rate Q (kW) and burning time t (s). The yield of combustion products was set as

0.113 for soot and 0.024 for carbon monoxide. In addition, the initial condition settings in the model were as follows: the temperature inside the station was 20℃, the pressure was 1.01×10^5 Pa, and the smoke concentration was 0 mol/mol.

$$Q = \alpha t^2 \tag{8}$$

The Large Eddy Simulation (LES) method has been performed better predictions in fire-induced smoke movement than the Reynolds averaging Navier–Stokes equation (RANS) and direct numerical simulation (DNS) (Ji et al., 2013). Based on the high efficiency in simulation process, the LES method was determined to use in this study. The Prandtl number (Pr) and the Schmidt number (Sc) are two crucial parameters in the LES simulations. The suitable values of Pr and Sc are in the range of 0.2 to 0.7 in the current research (Li et al, 2021a). And a good consistency was obtained between the simulated results with the experimental data with Sc = 0.4 and Pr = 0.3. Thus, the values of Pr and Sc were determined in this work.
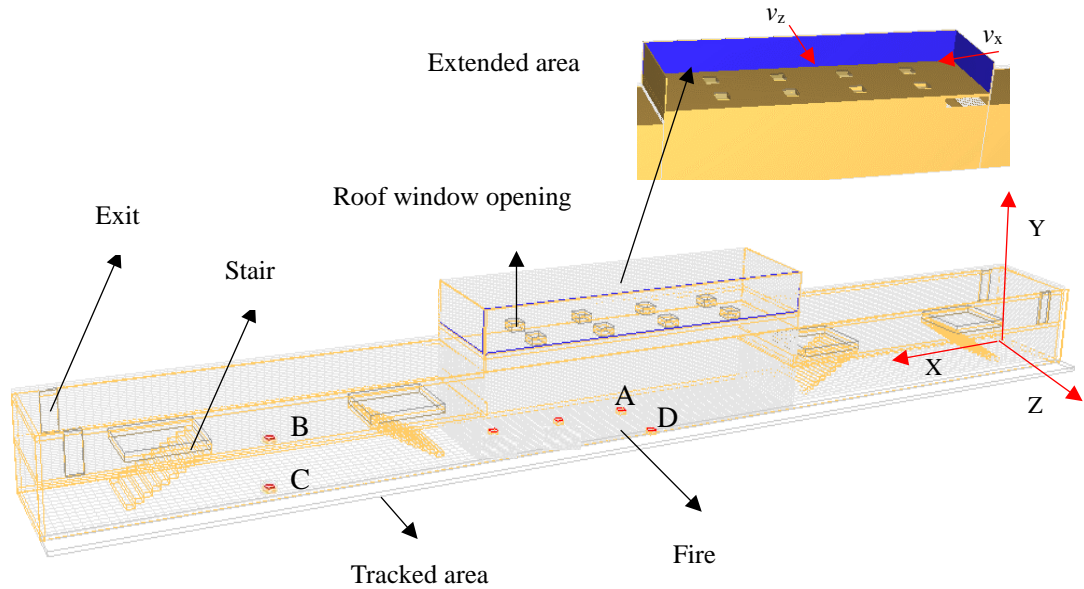

Fig. 6. Diagram of the numerical model.

4.3 Grid sensitivity analysis

The analysis of grid generation is a crucial step in the numerical simulation process. The grid size has a great influence on the accuracy of the results. For grid size design, the characteristic diameter D^* suggested in the FDS User Guide (Zhou et al., 2018) has been commonly adopted. And it was recommended that the appropriate value of D^*/x should range from 4 to 16. The definition of D^* can be expressed as:

$$D^* = \left(\frac{Q}{\rho_{in} c_p T_{in} \sqrt{g}} \right)^{2/5} \tag{9}$$

1 where D^* indicates the characteristic grid length; Q indicates the fire HRR; ρ_{in} indicates the ambient air

2 density; c_p indicates the specific heat capacity; T_{in} indicates the ambient temperature and g is the

3 gravitational acceleration.

4   In this work, four different gird sizes (0.1 m, 0.2 m ,0.25m ,0.5m) were adopted to analyze the grid

5 sensitivity. Former studies have confirmed that the grid is more sensitive near the fire source (the distance

6 is less than 40 m) than in other regions (Luo et al., 2014; Liu et al., 2019). Thus, the grid size in areas far

7 from the fire source (the distance is more than 40 m) was set to twice the size near the fire source. The

8 details of the grid sizes are shown in Table 2. Fig. 7 illustrates the change of smoke temperature and

9 velocity above the fire source with 2 MW for different gird sizes. On a reduced grid size of 0.5 m to 0.1

10 m, it is discovered that the temperature and velocity tend to be more accurate and consistent. For most

11 heights, the temperature value with grid sizes of 0.2 m and 0.1 m are in same range. And the velocity

12 curves with grid sizes of 0.2 m and 0.1 m also display remarkably close variation trend. It means the

13 increase of time-consuming in calculation cannot provide high accuracy of temperature values with the

14 reduction of mesh size from 0.2 m and 0.1 m. As a result, the grid system C, with grid sizes of 0.2 m ×

15 0.2 m × 0.2 m in the near the fire area and 0.4 m× 0.4 m × 0.4 m in the other regions, were applied in the

16 simulation work. The values of D^*/x were 12.66 near the fire area and 6.33 in other regions, with 1,214,24

17 total number of cells.
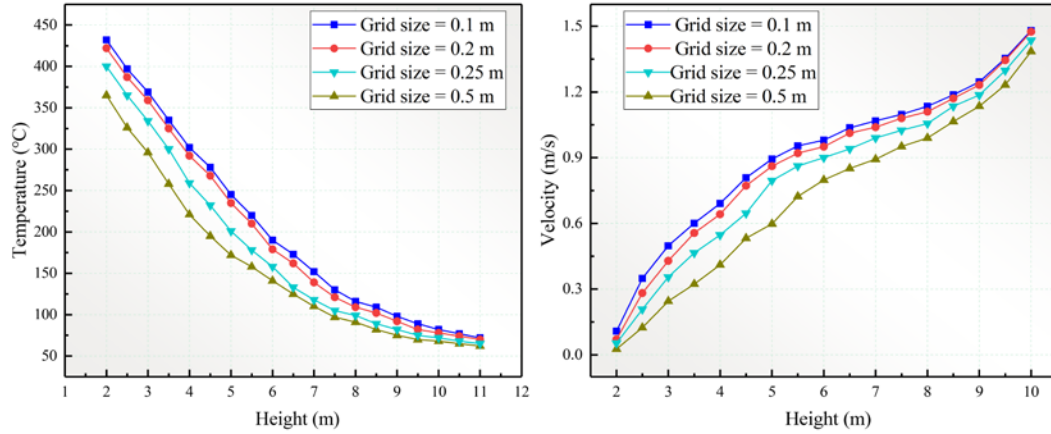
(a) Smoke temperature change above the fire   (b) Smoke velocity change above the fire

18

19   Fig. 7. Temperature and velocity change above the fire under a 2 MW fire for different grid sizes.

20   Table 2 Summary of grid system

Grid system	Grid Setting near Fire Source			Grid Setting in other Regions		
	δx (m)	δy (m)	δz (m)	δx (m)	δy (m)	δz (m)
A	0.1	0.1	0.1	0.2	0.2	0.2
B	0.2	0.2	0.2	0.4	0.4	0.4
C	0.25	0.25	0.25	0.5	0.5	0.5
D	0.5	0.5	0.5	1.0	1.0	1.0

21 **4.4 Verification of FDS modeling**

22   To assess the reliability of smoke movement by using FDS numerical simulation, the simulated results

1   of FDS were compared with the full-scale experimental results. A 1:1 subway model was established and

2   the structure and environmental parameters were consistent with the full-scale tests. The temperature

3   data, from the String#5 in No. 1 and No .2 tests, were adopted to verify the accuracy of simulation results,

4   as shown in Fig. 8. It is found that the simulation results of the temperature above the fire are slightly

5   higher than that from full-scale test. This is probably due to the difference in heat loss between the hot

6   smoke and the surface of the subway structure. The interior surfaces of the actual subway station are

7   decorated with lining, which have better heat absorption. While the interior surfaces in the FDS

8   simulation were set to concrete, which has poor heat absorption, resulting in high temperature. However,

9   the difference is very small and acceptable. Thus, it is reasonable to calculate the smoke parameters of a

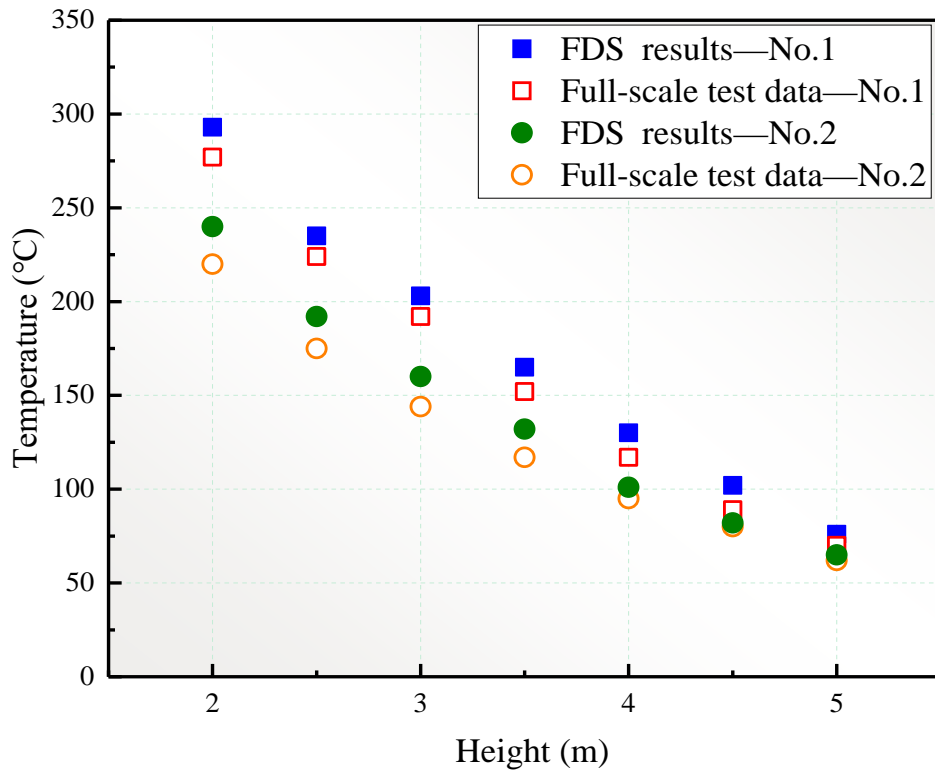10   subway fire by using the FDS numerical software.

12   Fig. 8. Temperature change above the fire source in full-scale tests and simulations

13   **4.5 Design of fire scenario conditions**

14   In a metro station fire, the factors affecting the smoke movement can be divided into three main

15   categories, such as the metro station configuration (ventilation pattern, space dimensions), the fire source

16   (fire location, HRR) and environmental conditions (air temperature, air velocity) (Gao et al., 2012a,

17   2012b; Meng et al., 2014). Orthogonal experimental design (OED), a highly efficient and accessible

18   multi-factorial experimental design method, which has been successfully employed in many research

19   areas (Tang et al., 2016; Xi et al., 2019; Zhang et al., 2021). The key to the OED method is making an

20   orthogonal design table based on reasonable levels of relevant factors. It could effectively reduce the

1 number of test cases by selecting representative factors (Ji et al., 2014; Li et al., 2020).

2 In order to screen the important factors affecting the smoke extraction efficiency of atrium metro

3 stations under fire scenario, a four-factor (fire HRR, atrium height, outdoor air temperature, outdoor air

4 velocity) and four-level orthogonal table L16 (4^4) was firstly designed (Zuo et al., 2016). And the

5 significance analysis of the influential factors was conducted in Statistical Product Service Solutions

6 (SPSS) software to obtain the sum of squared deviations of the errors (Se), statistical value of the F-test

7 (F) and significance value (P) (Zhan et al., 2023). As evident from Table 3, for the statistical value of the

8 F-test: $F_a > F_c > F_b > F_d$, and for significance value: $P_d > P_b > P_c > P_a$. While a higher P-value indicates

9 a smaller effect of the factor on the result. Hence, the influence factor levels of smoke extraction

10 efficiency were determined, the effect of fire HRR (factor a) was the largest, followed by outdoor air

11 temperature (factor c) and the atrium height (factor b), and the effect of outdoor air velocity (factor d)

12 was the least.

13 Table 3. Significance analysis of influential factors

Factors	Levels	S_e	F	P
a: Fire HRR (MW)	2/3/4/5	4213.16	26.33	0.012
b: Atrium height (m)	10/11/12/13	455.32	2.85	0.207
c: Outdoor air temperature (℃)	-20/0/20/40	986.14	6.16	0.085
d: Outdoor air velocity (m/s)	0.5/1.0/1.5/2.0	51.62	0.32	0.81

14 According to the results of the orthogonal experimental table L16 (4^4), as the P-value of the factors

15 generally exhibited insignificant effects (P > 0.100), the effects of the atrium height and outdoor air

16 velocity could be neglected with respect to the smoke extraction in subway fire scenario. And the minimal

17 impact was found on smoke extraction at atrium height of 12 m and outdoor air velocity of 0.5 m/s. Thus,

18 the values of these two factors were fixed in the following simulation conditions. Different fire locations

19 were developed into the subway fire scenario, and the details of fire scenarios in numerical simulation

20 are presented in Table 4.

21 Table 4. Summary of numerical scenarios.

Scenario number	Fire location	Atrium height H (cm)	Outdoor air velocity v_x and v_z (m/s)	Outdoor air temperature T_{out} (℃)	Fie HRR (MW)
A01-A35	A			-20/-10/0/10/20/30/40	1/2/3/4/5
B01-B07	B	12	0.5	-20/-10/0/10/20/30/40	2
C01-C07	C			-20/-10/0/10/20/30/40	2
D01-B07	D			-20/-10/0/10/20/30/40	5

22 **5.Results and discussion**

23 **5.1 Full-scale tests**

24 Figs. 9 - 11 show the full-scale experimental fire scenes in winter and summer of No.1 — No.6 tests.

25 After ignition, the fire develops upward in an axisymmetric plume. And the fire mixes with the smoke

from the smoke generator and striking upwards against the roof of the protective rack. Then the smoke enters into the common area. As can be clearly observed in Figs. 9a and 9b, the smoke spread in the common areas of the atrium fire is more extensive in winter condition than in summer condition. It is due to the inside temperature T_{in} is higher than outdoor air temperature T_{out}. The pressure difference $\rho_{in} < \rho_{out}$ results in the buoyancy momentum f_b higher than the gravitational force f_g, causing the outside air enter the station through the top roof openings. Thus, it is difficult for the smoke to escape from the top vents and even blowing the smoke downwards at the early stage after fire, resulting in rapid diffusion in the common areas.

The temperature change measured at String#1 — 4 in full-scale experiments are shown in Fig. 12. It can be found that the temperature decreases with increasing height at 2 m measurement strings near the fire source. This is attributed to the lower thermocouples are closer to the fire source and thus are directly heated by it. As can be seen in the Figs. 12b and 12c, the temperature changes in the thermocouple strings for platform fire as well concourse fires, the smoke temperature around the fire source is lower in winter than in summer. This is a result of the temperature difference between the outside and the inside of the subway station (Bilyaz et al., 2021). Furthermore, the platform fire is more affected by the natural smoke exhaust from the atrium, causing a greater temperature difference between the test No. 5 and No. 6 than the concourse fire experiments No. 3 and No. 4 (Long et al., 2020). For an atrium fire, the smoke temperature at the measurement points below 4 m height is higher in summer than that in winter. However, once the measurement point is above 4 m, the smoke temperature is higher in winter. The cold outside air enters the station through the natural openings at the top of the atrium, inhibiting the spread of smoke in the vertical direction. This causes an accumulation of smoke, resulting in a rise in temperature.

Figs. 13 show the smoke temperature above the fire source (String#5) and above the atrium (String#6) in the full-scale fire tests. It can be noticed that the temperature changes in the winter and summer seasons have the greatest effect on the atrium fires with 70 K temperature difference above the fire. While for concourse and platform fires, the temperature difference is below 30 K. With hybrid ventilation, station concourse and platform fires mainly depend on mechanical ventilation. In the case of atrium fires, the pressure due to the temperature difference between the outside and inside would have a significant impact on smoke extraction as fire source is directly below the natural smoke vent at the top (Xie et al., 2023).

(a) Test No.1 in winter   (b) Test No.2 in summer

Fig. 9. Full-scale experimental atrium fire scenes in winter and summer.

(a) Test No.3 in winter   (b) Test No.4 in summer

Fig. 10. Full-scale experimental concourse fire scenes in winter and summer

(a) Test No.5 in winter   (b) Test No.6 in summer

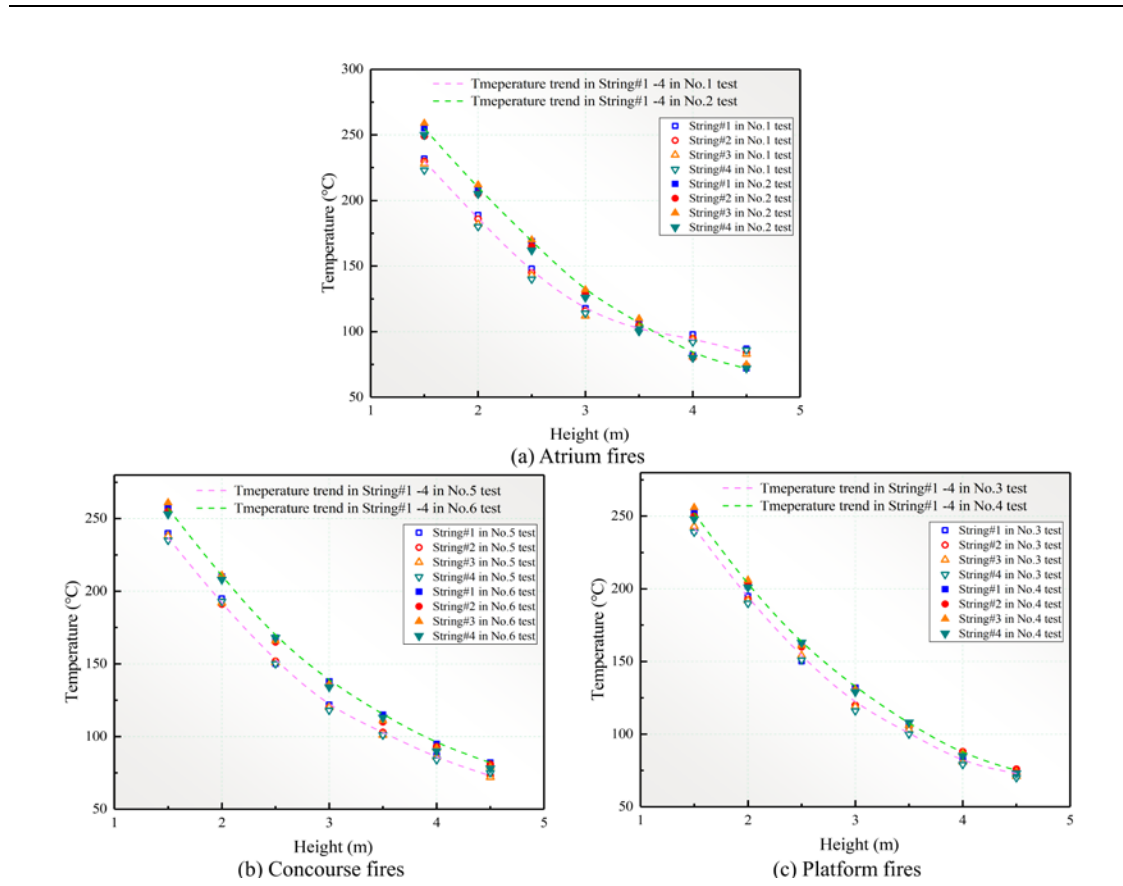Fig. 11. Full-scale experimental platform fire scenes in winter and summer

(a) Atrium fires

(b) Concourse fires

(c) Platform fires

Fig. 12. Temperature change of String#1 — 4 under different fire scenes in winter and summer.

(a) Temperature values of String#5

(b) Temperature values of String#6
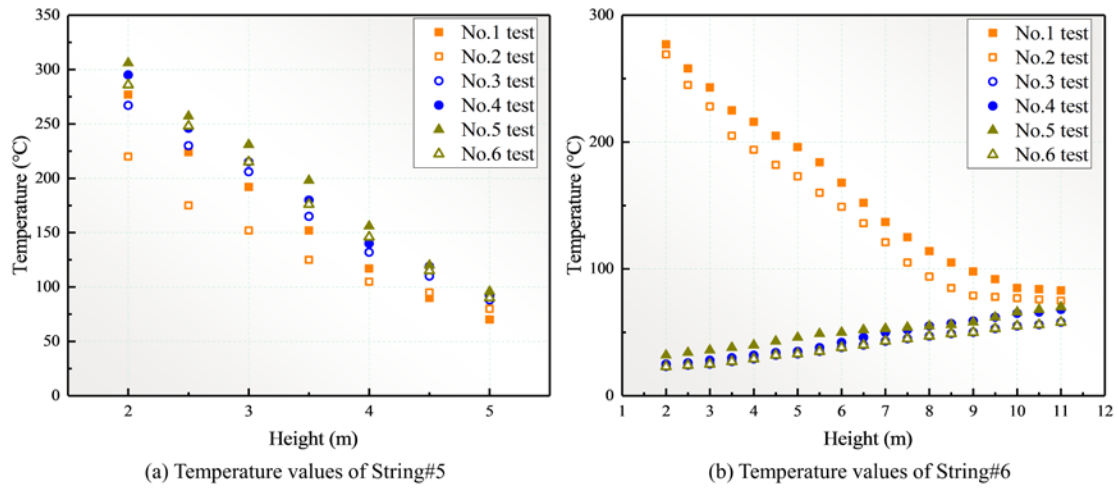
Fig. 13. Temperature change of String#5 and 6 in full-scale experimental tests.

5.2 Vertical temperature profile

Fig. 14 presents the smoke temperature variation above the fire source with outside temperature under different fire scenarios. It can be noticed in Fig. 14a that as the outdoor temperature decreases, the temperature above the 2 MW atrium fire decays faster. The difference in temperature decay above the fire is small when $T_{out} > 10°C$. Whereas for $T_{out} < 10°C$, the cold air entering the station would rapidly reduce the smoke temperature due to the large difference with the inside temperature of 20°C. The

19

nephogram of the temperature distribution directly above the fire is depicted in Fig. 15. It can be clearly

seen that the vertical temperature gradient increases as the outside temperature rises. While for concourse

fire (fire location B) and platform fire (fire location C), the variations in external temperature have little

effect on the smoke temperature the above the fire source, as shown in Figs. 14b and 14c. Taking an

example in Fig. 14c, the temperature difference at 3 m height above the fire source is less than 25°C by

comparing the cases of T_{out} = -20°C and T_{out} = 40°C. While for atrium fires in Fig. 14a, the temperature

difference is more than 70 K in the same cases. It is attributed to the long horizontal distance from the

fire source to the natural smoke vents at the top of the atrium. The cold air entering the station is difficult

to have an impact on the smoke in the vicinity of the fire source. Mechanical smoke extraction plays a

dominant role in the smoke propagation from concourse fires at long distance to the atrium, as well the

platform fires (Long et al., 2023). Fig. 14d shows the smoke temperature profile of 5 MW train fires (fire

location D). The maximum smoke temperature could reach 900°C and the smoke temperature above the

fire decreases quickly with the vertical height. While the variation of outside temperature has little

influence on smoke temperature as the train fire happened in the tracked area. Although the platform

screen doors are opened to diffuse smoke, the main part of the smoke is exhausted via mechanical exhaust

from the rail top (Shi et al., 2021).

(a) 2 MW atrium fire

(b) 2 MW concourse fire

(c) 2 MW platform fire
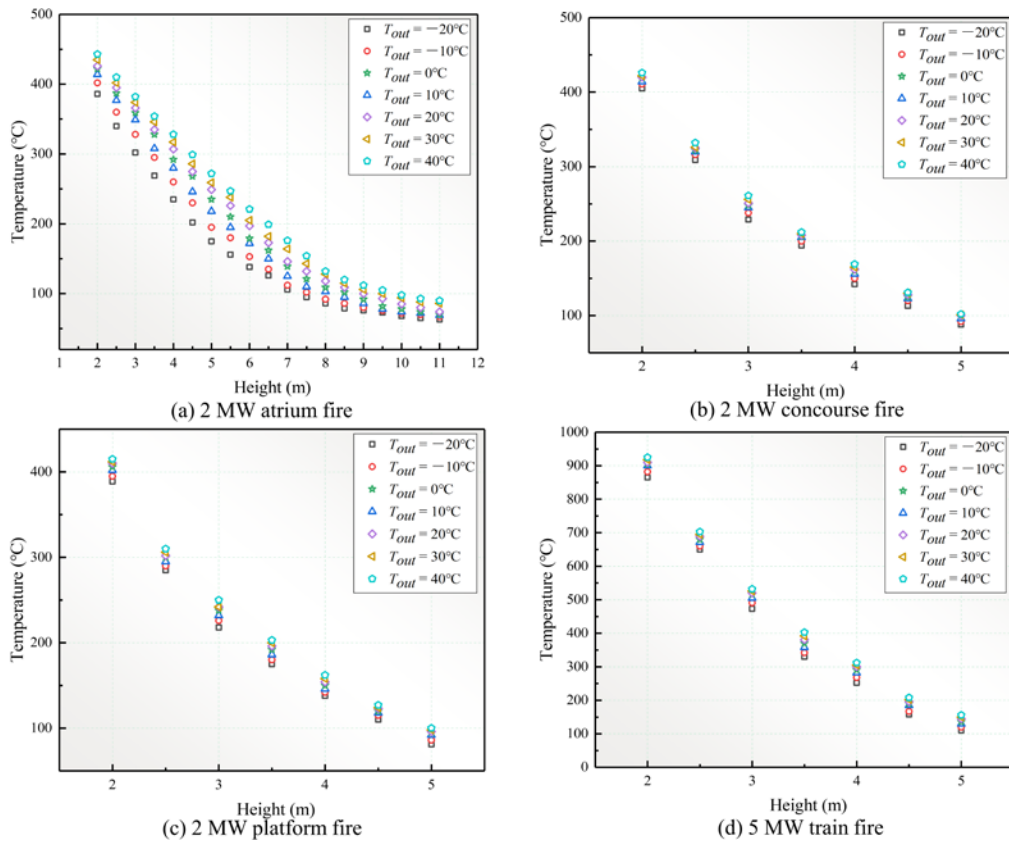
(d) 5 MW train fire

Fig. 14. Vertical smoke temperature profile with outside temperature
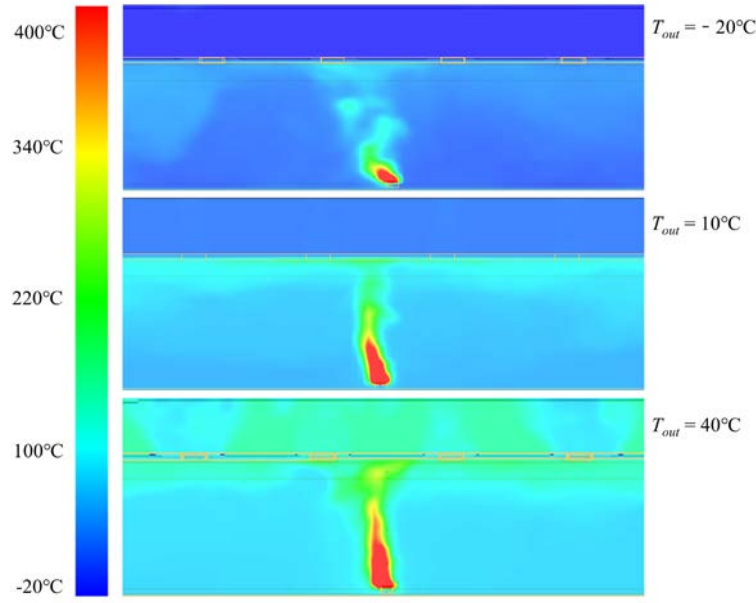
under different fire scenarios

Fig. 15. Nephogram of the temperature distribution with outside temperature

under 2 MW atrium fires.

The fire HRR has a significant impact on the temperature distribution in the station. Fig. 16 shows the smoke temperature rise $\Delta T = T_s - T_{in}$ beneath the atrium ceiling with various HRRs in fire location A. It is obvious that the temperature decay presents a top-hat distribution. The maximum value occurs at the peak of hat, consistent with the results of Pan's work (Pan, et al, 2022). The non-dimensional temperature rise $\Delta T / \Delta T_{max}$ and vertical height from the floor surface z/H were employed to unify the temperature profile (Oka and Imazeki, 2014a, 2014b, 2015):

$$\frac{\Delta T}{\Delta T_{max}} = C_1 (\frac{z}{H} + C_2) \cdot \exp(C_3 \frac{z}{H}) \tag{10}$$

where C_1, C_2, C_3 and C_3 are the coefficients to be determined by nonlinear analysis.

According to the measured data obtained from numerical works, the normalized temperature distributions for each outdoor temperature are calculated by Eq. (10), as shown in Fig. 17. It is obvious that the normalized temperature distributions are independent of the heat release rate, consistent with the results of Oka and Pan (Oka and Imazeki, 2015; Pan, et al, 2022). Besides, the influence due to the outdoor temperature can be observed. The bulging shape of the normalized temperature distributions shrinks with the increase of the outdoor temperature. As the T_{out} ranges from -20°C to 40°C, the temperature gradient trend of $\Delta T / \Delta T_{max}$ at the ceiling fluctuates slightly. This phenomenon is similar to the Oka's work (Oka and Imazeki, 2015). While the temperature trend is smoothest under $T_{out} = 10$°C. It is concluded that the value of $\Delta T / \Delta T_{max}$ decreases with a range of $0 < z < H$ with the characteristic position z/H.
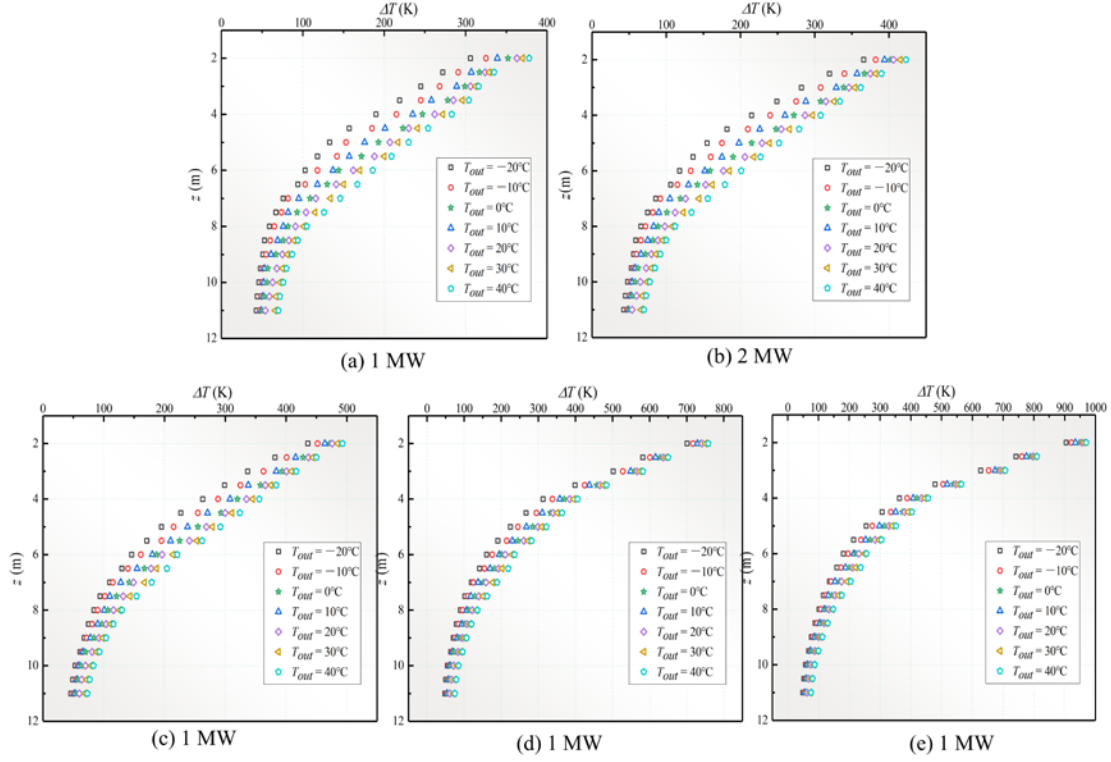
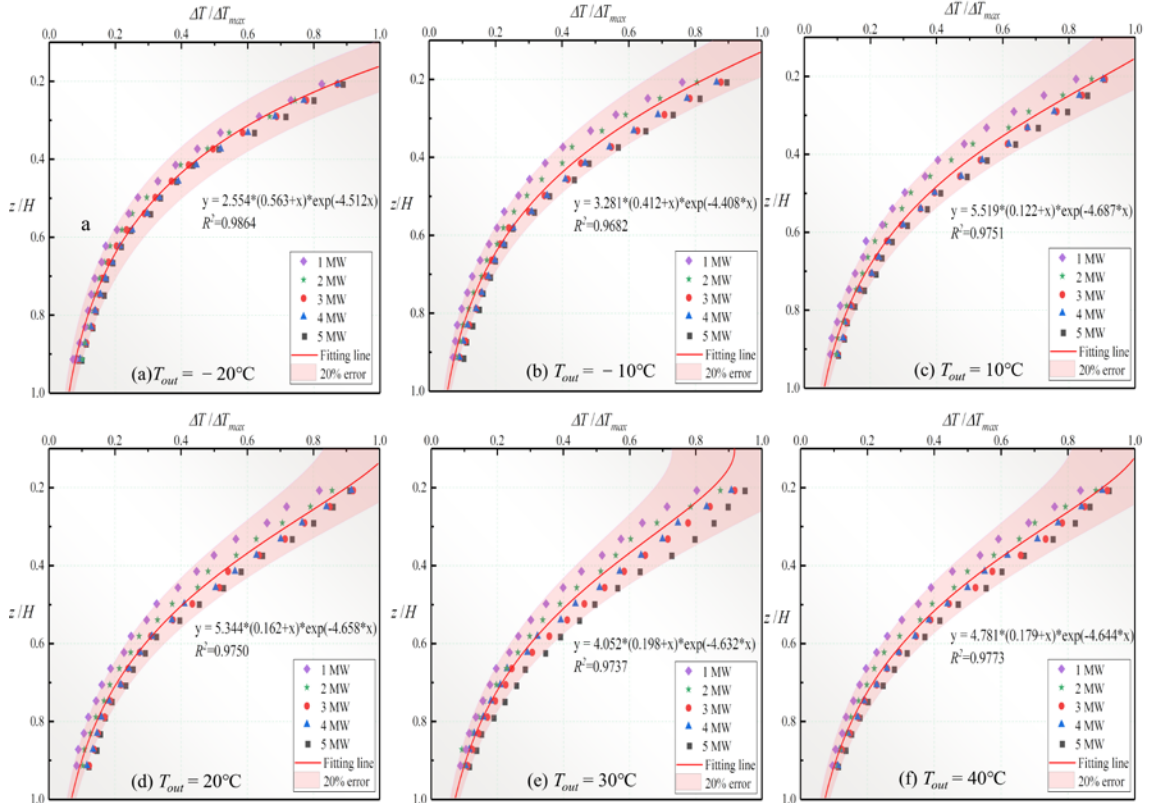Fig. 16. Vertical smoke temperature profile with different HRRs under atrium fire.

Fig. 17. Normalized temperature distributions with each outside temperature.

In Eq. (10), C_1, C_2, and C_3 are determined by the nonlinear analysis and almost all the data are within 20 % relative error (red region in Fig. 17). Table. 5 shows the detailed coefficients. It can be found that

1   the coefficients are dependent on outdoor temperature. And the favorable outdoor temperature T_{fav} for

2   vertical temperature decay is defined as 10°C. Due to the temperature difference between outside and

3   inside of the station, the outside temperature could be divided into two regions: Region I (T_{out} <10°C)

4   and Region II ($T_{out} \geq$ 10°C). The variation trend of the coefficients with the outside temperature is

5   reflected in Fig. 18. The feasibility of this study on the temperature profile above the fire through the

6   definition of the characteristic outdoor temperature is proven. Based on the red fitting lines in Fig. 18,

7   the values of C_1, C_2, and C_3 in Region I and Region II are described as follows:

8
$$\begin{cases} C_1 = 0.101 \cdot (T_{fav} - T_{out}) + 5.60 \\ C_2 = 0.014 \cdot (T_{fav} - T_{out}) + 0.13 \\ C_3 = 0.017 \cdot (T_{fav} - T_{out}) - 4.68 \end{cases} \qquad \text{Region I: } T_{out} < T_{fav} \quad (11)$$

9   and

10
$$\begin{cases} C_1 = -0.005 \cdot (T_{out} - T_{fav}) + 5.60 \\ C_2 = 0.002 \cdot (T_{out} - T_{fav}) + 0.13 \\ C_3 = 0.002 \cdot (T_{out} - T_{fav}) - 4.68 \end{cases} \qquad \text{Region II: } T_{out} \geq T_{fav} \quad (12)$$

11   By combining Eqs. (10), (11) and (12), normalized vertical temperature distributions above the floor

12   in terms of outdoor temperature can be expressed as:

13
$$\begin{cases} \frac{\Delta T}{\Delta T_{max}} = \left\{ \left[0.101 \cdot (T_{fav} - T_{out}) + 5.60 \right] \right\} \\ \quad \left\{ \left[0.014 \cdot (T_{fav} - T_{out}) + 0.13 \right] + \frac{z}{H} \right\} \\ \quad exp \left\{ \left[0.017 \cdot (T_{fav} - T_{out}) - 4.68 \right] \frac{z}{H} \right\} \end{cases} \qquad \text{Region I: } T_{out} < T_{fav} \quad (13)$$

14   and

15
$$\begin{cases} \frac{\Delta T}{\Delta T_{max}} = \left\{ \left[-0.005 \cdot (T_{out} - T_{fav}) + 5.60 \right] \right\} \\ \quad \left\{ \left[0.002 \cdot (T_{out} - T_{fav}) + 0.13 \right] + \frac{z}{H} \right\} \\ \quad exp \left\{ \left[0.002 \cdot (T_{out} - T_{fav}) - 4.68 \right] \frac{z}{H} \right\} \end{cases} \qquad \text{Region II: } T_{out} \geq T_{fav} \quad (14)$$

16   Since the empirical model is established with outside temperature from -20°C to 40°C. As clearly shown

17   in Fig. 19, the comparison of the predicted values by Eqs. (13) and (14) with full-scale experimental

18   results and other full-scale experiments (Long et al., 2020; Liu et al., 2020 and Liu et al., 2022). The

19   predicted values are almost consistent with the experimental results and the error range is less than 10%.

20   However, it should be noticed that the calculated values by empirical model are smaller than some of the

21   experimental results, such as the full-scale platform and concourse fires, experiments in Liu's works (Liu

22   et al., 2020; Liu et al., 2022). It is attributed to the fact that the prediction model takes full account of

23   outside temperature factor. While the platform and concourse fires are far from the natural openings on

24   the atrium roof, both in this work and previous work. The variation of outside temperature has little

25   influence on the fire and temperature distribution. In addition, Long's experiments were conducted in a

26   double-island subway station under hybrid ventilation. The total height of the metro station is 11 m,

which is similar to the size of station in this work. From comparison, the data of full-scale fire experiments in Long's work consistent with the predicted values. Based on the good agreement, it sufficiently demonstrates that the empirical model is applicable as an engineering tool for huge and tall buildings with natural exhaustion.

Table .5 Determined values of coefficients at each outdoor temperature.

Outdoor temperature (°C)	C_1	C_2	C_3
-20	2.554	0.563	-4.152
-10	3.281	0.412	-4.408
0	4.544	0.294	-4.569
10	5.519	0.122	-4.687
20	5.344	0.162	-4.658
30	4.781	0.179	-4.644
40	4.052	0.198	-4.632
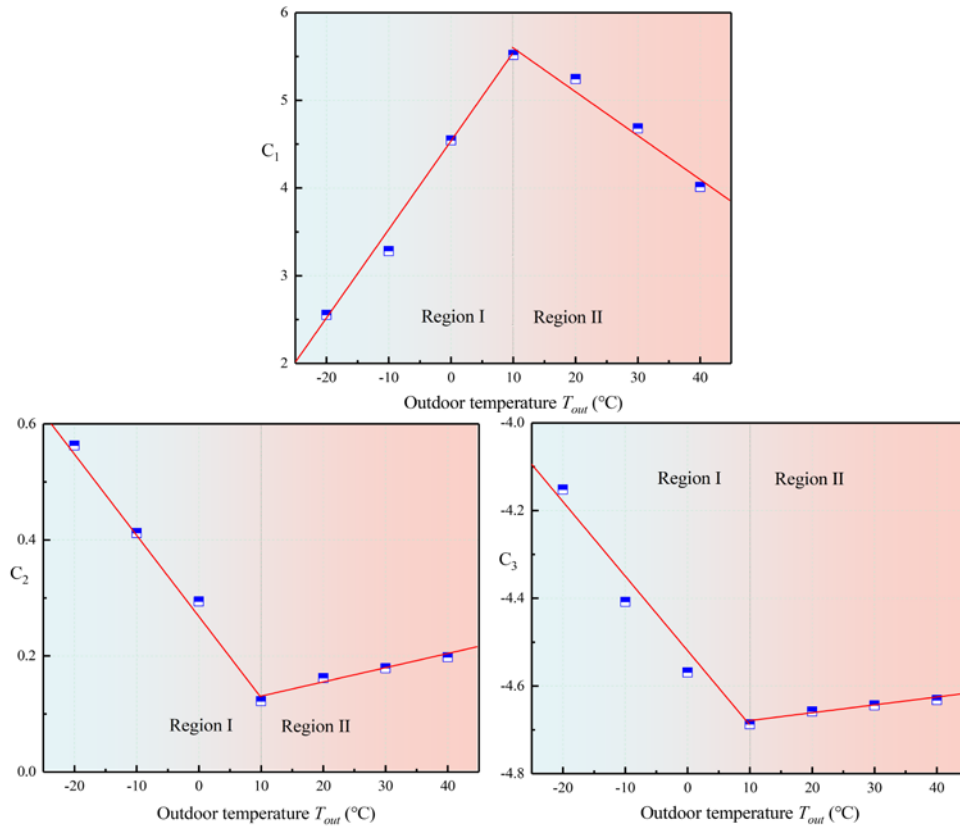
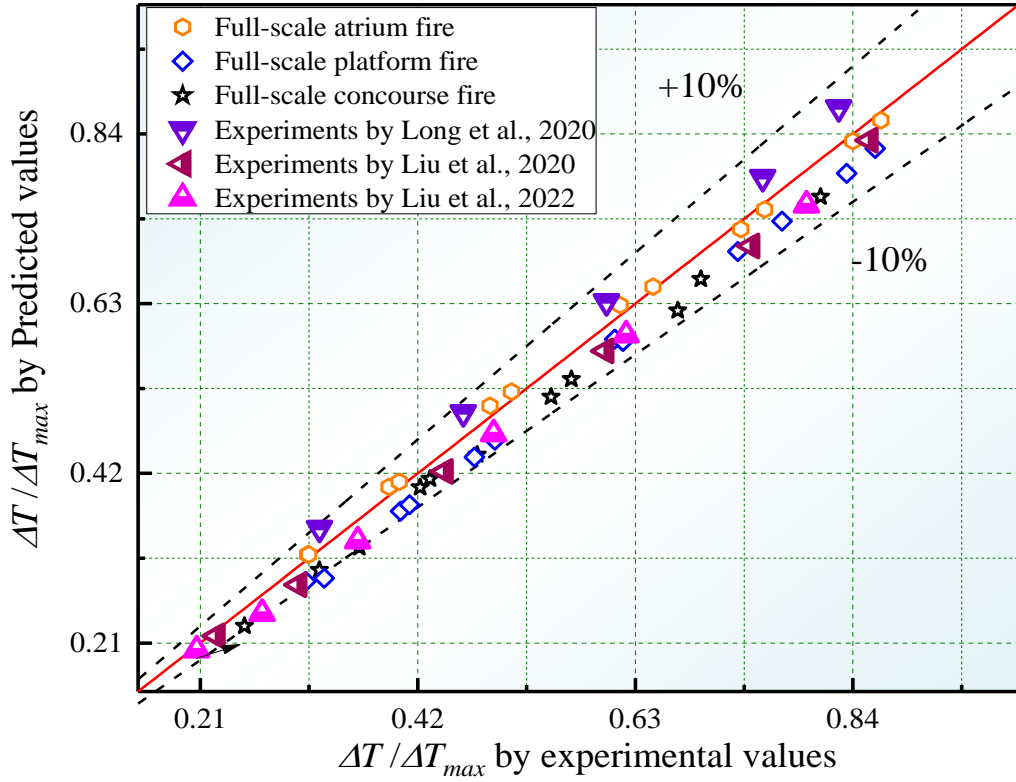Fig. 18. Fitting lines of coefficients with varying of outdoor temperature

Fig. 19. Comparison of the dimensionless flame height among the predicted model, experimental results, and previous data.

5.3 Smoke movement

Fig. 20 presents the smoke movement with different outdoor temperature under 2 MW atrium fires at 20s, 50s, 120s and 240s. It can be obviously seen that the outdoor temperature has a significant influence on fire smoke propagation. At the early 50s after fire, the smoke can hardly escape from the natural openings on the top roof of the station under the conditions outdoor temperature are -20℃ and 10℃. Especially, smoke mainly descends to near ground height as the outdoor temperature is -20℃. While the smoke flow smoothly out of the natural opening when the outside temperature is 40 ℃. Based on the Eq. 4, once the smoke layer height h_{sm} is 12.0 m, the $\frac{dT}{dz}$ could be calculated by the formula Eq. 14 and determined as 2.4 K/m (Beyler et al., 1995). Thus, the smoke can reach the top of the atrium as long as the outside temperature is below 48.8℃. It indicates that high outside temperature ($T_{out} < 48.8℃$) is beneficial to smoke exhaust at the initial stage after fire. And the cold outside environment makes the smoke drop rapidly, causing difficulties in evacuating people (Bilyaz et al., 2021).
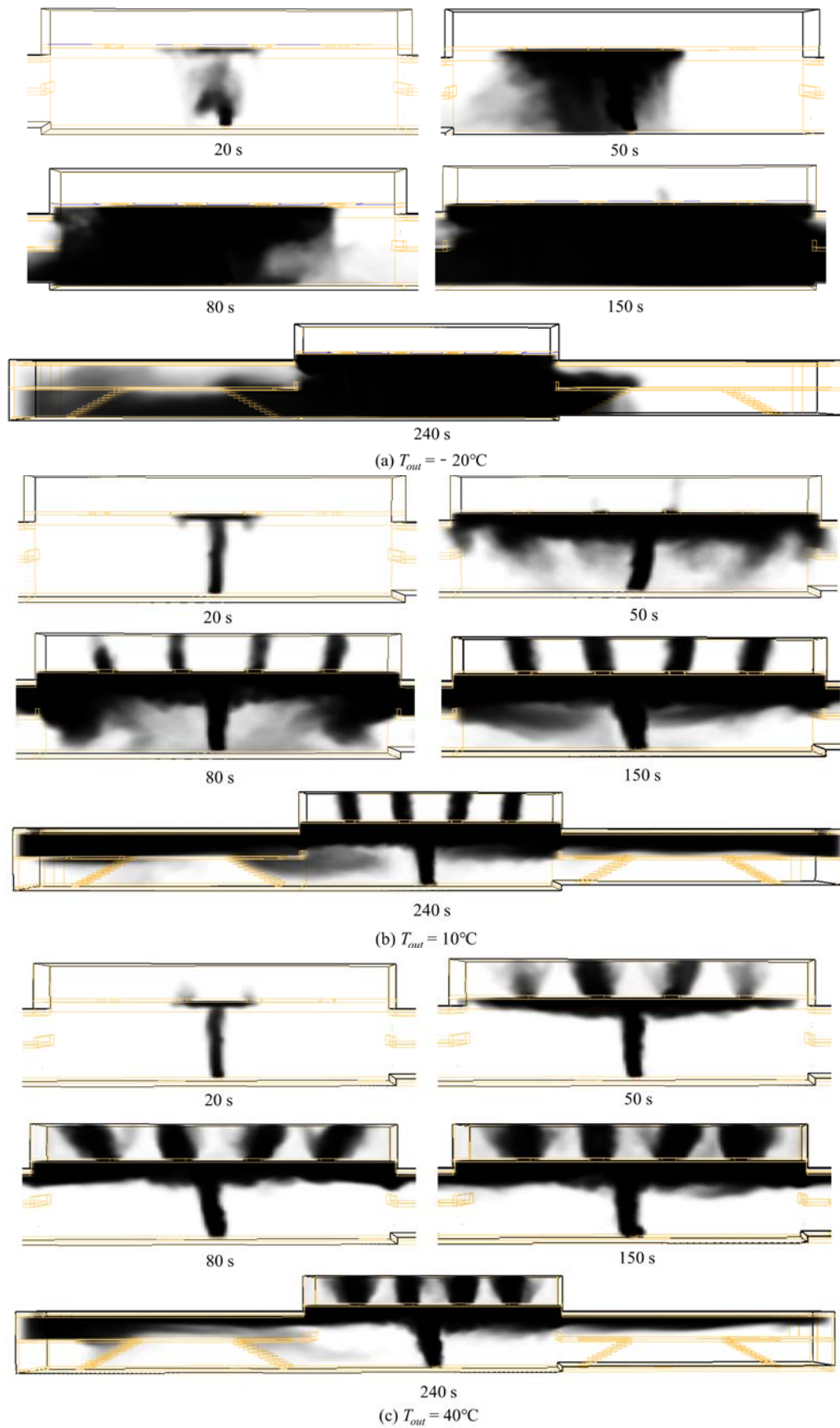
$$\frac{dT}{dz} = \left[\frac{3.79}{h_{sm}} \sqrt{\frac{T_{in}}{g(\rho c_p)^2}}^{1/8} Q_c^{1/4} \right]^{8/3}$$

(14)

After 80 s of the fire in Fig. 20a, smoke gradually spread in the horizontal direction under $T_{out} = $ -

20°C.The smoke layer is close to the ground and most smoke spreads into the platform. At 150s, smoke has already filled with the atrium space and still not be exhausted from the top openings (Krol et al., 2017). While the some could escape from the natural openings at 80 s when outside temperature is 10°C, as shown in Fig. 20b. Although the smoke can be exhausted through the natural and mechanical smoke vents, smoke has almost occupied the concourse space at 240 s. The smoke layer height has descended to the concourse floor when $T_{out} = 10$°C. According to Eq. 15, the minimum outside temperature is estimated as 10°C which can meet $A_r > 1$ in the case of inside temperature is 20°C. It indicates that once the $T_{out} < 10$°C, the $A_r < 1$ and the smoke cannot escape from the natural openings.

$$T_{out} = \frac{\Delta T_{os}}{Ar} g - 273$$
(15

The large temperature difference between cold outdoor temperature and indoor environment causes the "reverse stack effect". The airflow is from outside to the internal through the top openings at 50 s, as shown in Fig. 21. However, the velocity direction is from inside to the outside under $T_{out} = 10$°C and 40°C. Fig. 22 gives the airflow velocity through the top openings with time. The velocity increases with the outdoor temperature rises. And it can be observed that as the T_{out} changes from -20°C to 10°C, the velocity various largely from around -3.5 m/s to 1.5 m/s. While the outside temperature exceeds 20°C, the vertical velocity through the natural openings only has a smaller change. It is attributed the density difference between the outside and inside environment. As the thermal buoyancy is greater than the gravitational force of the outside air, the smoke flows out of the top openings (Ahn et al., 2020). And the greater the thermal buoyancy, the larger the outflow velocity.

20 s

50 s

80 s

150 s

240 s

(a) T_{out} = - 20°C

20 s

50 s

80 s

150 s

240 s

(b) T_{out} = 10°C

20 s

50 s

80 s

150 s

240 s

(c) T_{out} = 40°C

Fig. 20 Smoke movement with different outdoor temperature under 2 MW atrium fires
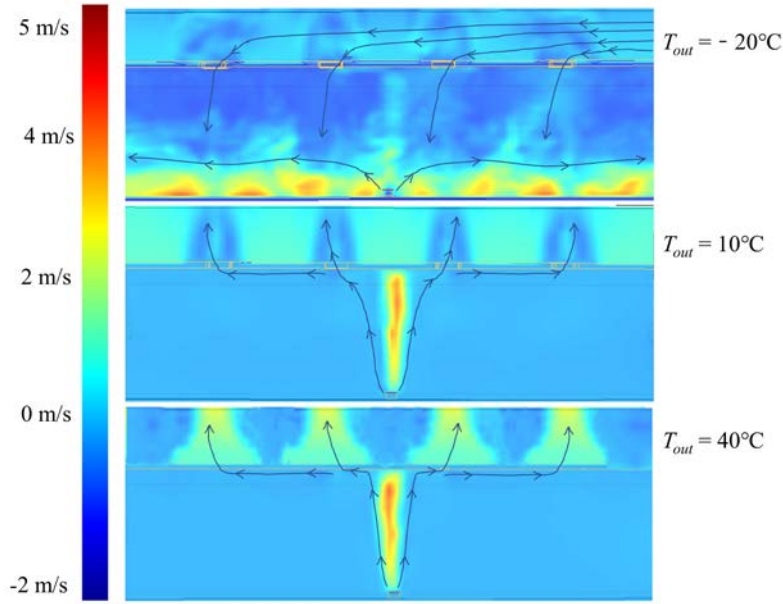
1
2

1

2   Fig. 21 Smoke velocity with different outdoor temperature under 2 MW atrium fire at 50 s
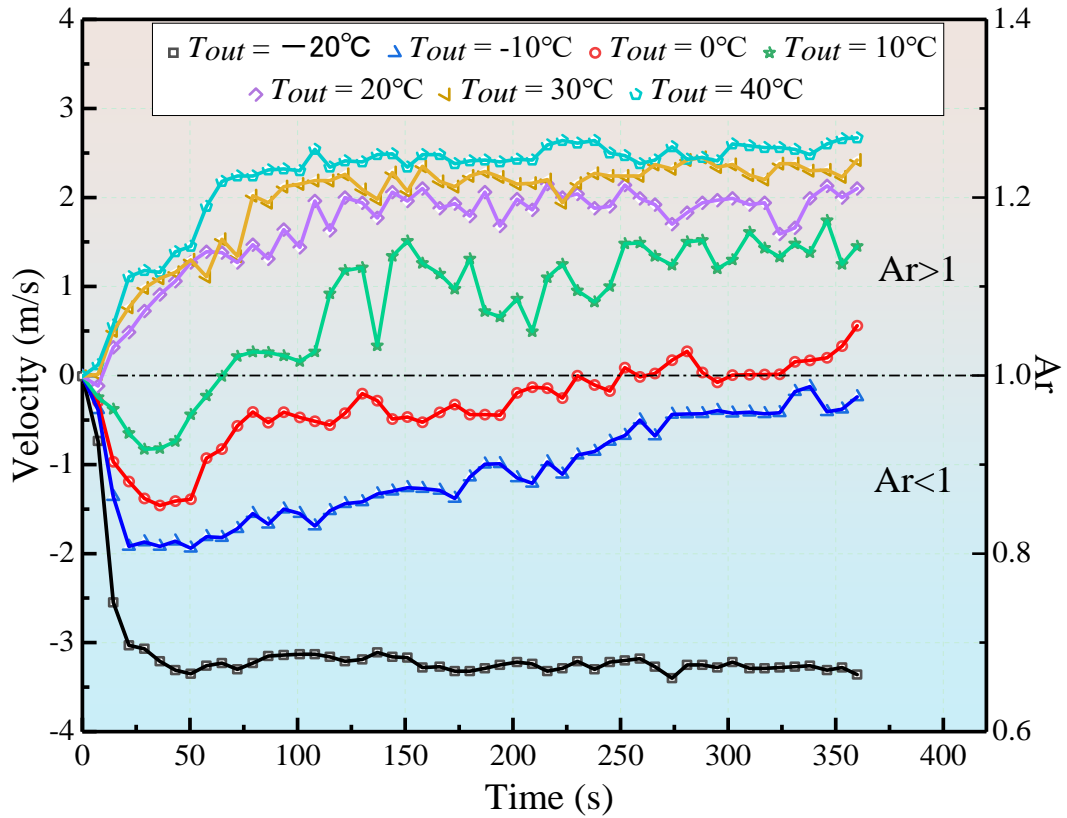

3

4   Fig. 22. Airflow velocity through the top opening with time under 2 MW atrium fires.

5 **5.4 Smoke extraction efficiency through natural openings**

6   The volume of the CO concentration exhausted from the roof openings ($CO_{natural}$) is significantly

7 influenced by the outdoor temperature, see Fig. 23. As the outdoor temperature below 10°C ($A_r < 1$), the

CO concentration is lower than 50 ppm and nearly to 0 ppm in most of time. While with the T_{out} varies 10°C to 40°C ($A_r > 1$), the $CO_{natural}$ changes from 300 ppm to 500 ppm. The higher the outdoor temperature is, the more CO will be exhausted from the top natural openings.

The smoke exhaustion efficiency through natural exhaustion is calculated by the following equation (Zhang et al., 2021):

$$\eta = \frac{m_{natural}}{m_{total}} = \frac{CO_{natural}}{CO_{total}} \tag{16}$$

where η is the smoke exhaustion efficiency through natural exhaustion, $m_{natural}$ is the volume of smoke exhausted from the roof openings, m_{total} is the total volume of smoke produced by the fire, $CO_{natural}$ is the volume of CO concentration exhausted from the roof openings, CO_{total} is the total volume of CO concentration produced by the fire.

Fig. 24 depicts the values of η with different outdoor temperature under fire scenarios. It can be observed that with the outdoor temperature increases, the smoke exhaustion efficiency shows a growth trend. For example, under 2 MW atrium fire, the η could reach 30% at outside temperature is 40°C, while nearly 0% of the -20°C and -10°C. It means that more smoke will be exhausted through the ceiling vent by the natural exhaustion way under higher outdoor temperature conditions ($A_r > 1$). Based on this, the larger volume of the CO to be exhausted through the roof openings and thus lead CO exhaustion efficiency will be higher (Gao et al., 2015). The fire HRR also makes a positive effect on the smoke exhaustion efficiency. It is attributed to the larger fire results in higher smoke temperature (Tan et al., 2021). The upward momentum of the airflow buoyancy becomes greater and more smoke would be exhausted through the natural vents. Besides, by comparing the same HRR of the fire, it can be found that the outside temperature changes have the greatest impact on atrium fires. The fires occur at platform, concourse and tracked area are insensitive to the variation of the outdoor temperature. This is due to the top natural openings are far from the fire locations. And the mechanical exhaustion serves a major function after the fire.
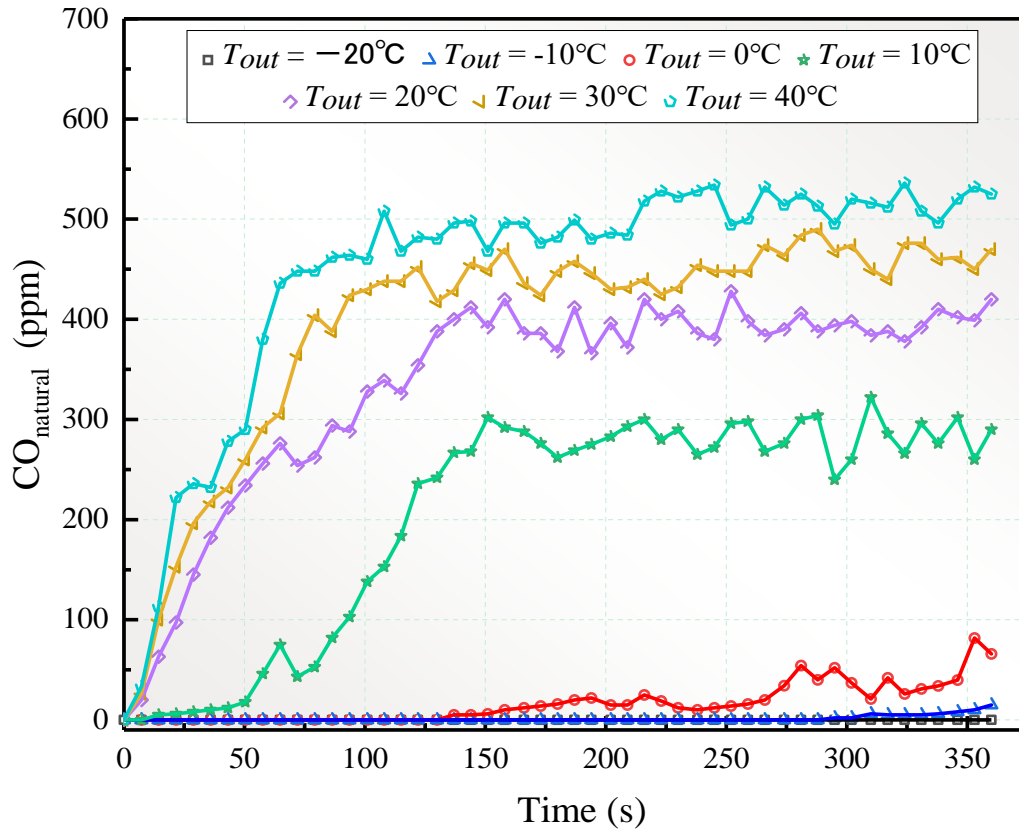
1

2   Fig. 23. CO concentration exhausted from the roof openings with time under 2 MW atrium fires.
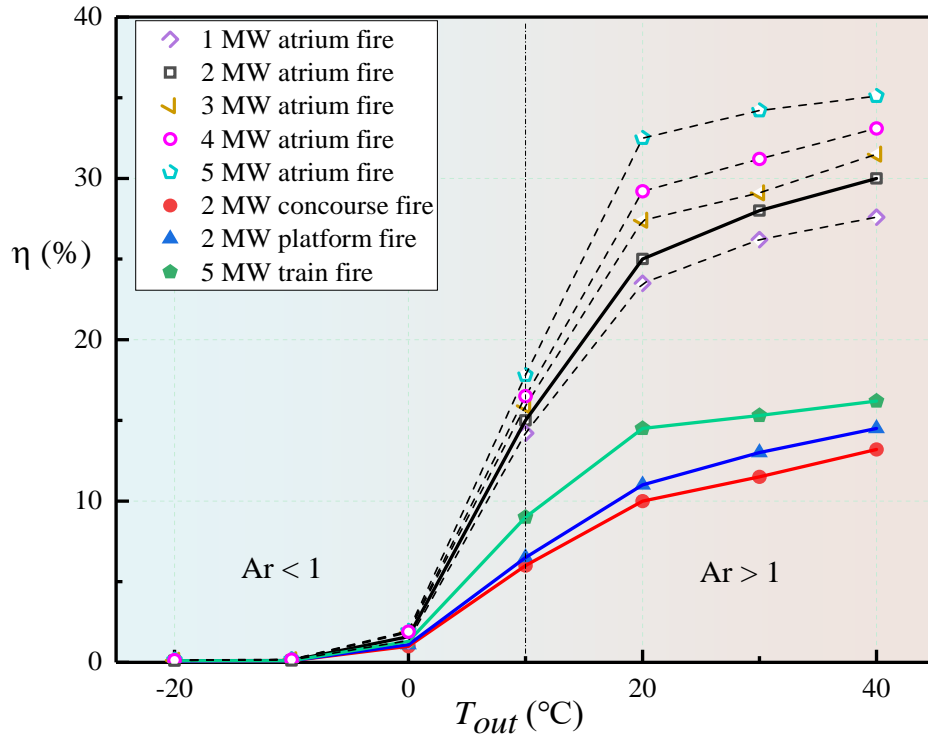

3

4   Fig. 24. Smoke exhaustion efficiency with different outdoor temperature under fire scenarios.

6.Conclusion

In the present work, the influence of outdoor environmental parameters on fire-induced smoke characteristics with hybrid exhaustion in atrium-type metro station were studied. Full-scale experiments were both conducted in winter and summer with different fire scenarios and a series of numerical simulation works were carried to investigate the detailed effects of outdoor environments based on the results of orthogonal experimental design table. The vertical temperature profile, smoke movement and smoke extraction efficiency through natural openings were analysed. Major findings can be drawn as follows:

(1) From full-scale experiments, it was found that the fire-induced smoke spread inside the metro station is more extensive in winter condition than in summer condition. The cold outside air in winter would enter the station through the natural openings at the top of the atrium, inhibiting the smoke diffusion vertically and contributing to horizontal propagation. The smoke temperature around the fire source was lower in winter than in summer. Note that the outdoor temperature changes in the winter and summer seasons have larger influences on atrium fires than the concourse and platform, with 70 K than 30 K in temperature difference above the fire. With hybrid ventilation, the smoke extraction of station concourse and platform fires mainly depend on mechanical ventilation.

(2) The vertical temperature gradient inside the atrium increases as the outside temperature rises from -20°C to 40°C. The temperature decay above the fire presented a top-hat distribution. And the normalized temperature distributions were found to be independent of the fire heat release rate, and the bulging shape of the distribution shrank with the increase of the outdoor temperature. The outside temperature was divided into two regions according to the temperature difference between outside and inside of the station. The empirical models were established to estimate the temperature profile taking the effect of outdoor temperature into consideration. The predicted values by the proposed model are almost consistent with the full-experimental results in this work and previous work with error range less than 10%.

(3) The outdoor temperature has a significant influence on fire smoke propagation inside the station. Especially in cold winter, the large temperature difference between cold outdoor temperature and indoor environment causes the "reverse stack effect". The airflow was from outside to the internal through the top openings after fire. According to the criteria value of Ar, the effect of the outdoor air temperature on the smoke movement was divided into two regions. The airflow velocity through the natural openings increases with the outdoor temperature rises. And it varies largely from around -3.5 m/s to 1.5m/s from -20°C to 10°C (Ar < 1). While for outside temperature exceeds 20°C (Ar > 1), the airflow velocity only has a smaller change.

(4) The higher the outdoor temperature is, the more CO would be exhausted from the top natural openings. As the outdoor temperature below 10°C ($A_r < 1$), the CO concentration exhausted from the natural openings was lower than 50 ppm and nearly to 0 ppm in almost time. While with the T_{out} varies 10°C to 40°C ($A_r > 1$), the $CO_{natural}$ changes from 300 ppm to 500 ppm. The fire HRR also makes a

positive effect on the smoke exhaustion efficiency. The upward momentum of the airflow buoyancy becomes greater and more smoke would be exhausted through the natural vents. Found that the changes of outside temperature have the greatest impact on atrium fires. The fires occur at platform, concourse and tracked area are insensitive to the variation of the outdoor temperature.

The results of the present study can provide guidance for the optimizing fire safety design and smoke control in metro stations. It should be emphasized that the results are applicable in the context of fire scenarios with external temperature ranging from -20°C to 40°C and fixed outdoor air velocity. The effects of outdoor air velocity and other factors on fire-induced smoke have initially discounted based on the orthogonal experiments. However, these factors can also have an impact on smoke movement. And the extreme weather conditions such as temperatures below -20°C or above 40°C should be considered in future studies. In conclusion, this research provides a significant contribution to the field of smoke control in metro stations. It highlights the need for ventilation design in this field to consider the changes of outdoor environment parameters in more complex scenarios.

Credit authorship contribution statement

Desheng Xu: Conceptualization, Data curation, Investigation, Software, Methodology, Validation, Formal analysis, Writing – original draft. Yan Feng Li: Conceptualization, Funding acquisition, Project administration, Resources, Supervision, Writing – review & editing. Tianmei Du: Investigation, Writing – review & editing. Hua Zhong: Writing – review & editing. Junmei Li: Methodology, Supervision. Jiaxin Li: Investigation, Writing – review & editing. Youbo Huang: Writing – review & editing.

Declaration of Competing Interest

The authors declare that they have no known competing financial interests or personal relationships that could have appeared to influence the work reported in this paper.

Data availability

Data will be made available on request.

Acknowledgements

Appendix. Uncertainty analysis

The accuracy of test instruments is the most important component in determining the uncertainty of experimental results. The root sum square (RSS) was developed to estimate the uncertainty results

in this work (Kline and Mcclintock, 1953). The calculating formula is written as follows by including the uncertainty originating from each element:

$$\delta R = \left(\sum_{i=1}^{N} \left(\frac{\partial R}{\partial X_i} \delta X_i \right)^2 \right)^{1/2} \tag{A1}$$

where δX_i is the contribution of each element's uncertainty; δR is the overall uncertainty.

(1) Uncertainty in the HRR measurement.

The mass loss method was used to measure the HRR in the full-scale experiments. The following formulae (A2) can be used to calculate the uncertainty of the HRR:

$$\frac{\delta \dot{m}}{\dot{m}} = \pm \left[\left(\frac{\partial \dot{m}}{\partial \Delta m} \frac{\delta \Delta m}{\Delta m} \frac{\Delta m}{\dot{m}} \right)^2 + \left(\frac{\partial \dot{m}}{\partial \Delta t} \frac{\delta \Delta t}{\Delta t} \frac{\Delta t}{\dot{m}} \right)^2 + \left(\frac{\partial \dot{m}}{\partial A} \frac{\delta A}{A} \frac{A}{\dot{m}} \right)^2 \right]^{1/2} \tag{A2}$$

where $\frac{\delta \Delta m}{\Delta m}$, $\frac{\delta \Delta t}{\Delta t}$ and $\frac{\delta A}{\Delta A}$ respectively represent the relative uncertainties of the measured mass loss, time interval, and pool surface size. The uncertainty of measured mass loss is mainly influenced by the accuracy of the mass flowmeter. The technical handbook states that the relative errors for all values are ±0.1 g, the time interval uncertainty of mass flowmeter is 0.5s, with 1mm uncertainty of the area of fuel pans. Substituting these uncertainty values into Eq. (A2), the relative uncertainty of the measured HRR in this work is less than ±9.0%.

(2) Uncertainty of the temperature measurement.

The fire experiments were all conducted under the ambient temperature around 15°C. The temperature was measured using a K-type thermocouple with an accuracy of 0.75% within a range of 0 to 1300°C. Thus, employing a conservative value of ±1°C, the relative uncertainty of temperature could be calculated as $\frac{\delta T}{T} = \pm \left(\frac{\pm 1^\circ C}{T^\circ C} \right)$. The maximum uncertainty of measured temperature is ± 5.0%.

(3) Uncertainty of the velocity measurement.

The average value of air velocity of a section taken at ground level is considered as the outdoor air velocity. A TSI high-precision miniature anemometer DP-CALC 8715 with an accuracy of ± 2% was used to measure the velocity. The uncertainty of $\bar{u}_0$ can be calculated by:

$$U_{\bar{u}_0} = \sqrt{ \sum_{i=1}^{5} \left(\frac{\partial \bar{u}_0}{\partial u_i} U_{u_i} \right)^2 } \tag{A3}$$

$$u_i = \frac{1}{n} \sum_{j=1}^{n} u_{i,j} \tag{A4}$$

where $u_{i,j}$ is the j th measured value of u_i, and n is the number of measurements of the i th measuring point. The uncertainty of the velocity in this study is less than ± 4%.

Reference

Ahn, C.S., Kim, D.Y., Park, C., Kim, M.W., Kim, T., Bang, B.H., An, S., Yarin, A.L., Yoon, S.S., 2020. Experimental and numerical study of smoke behavior in high-rise stairwells with open and closed windows, Int. J. Therm. Sci. 157, 106500.

Barbato, L., Cascetta, F., Musto, M., Rotondo, G., 2014. Fire safety investigation for road tunnel ventilation systems-an overview. Tunn. Undergr. Space. Technol. 43, 253-265.

Beijing Urban Construction Design & development Group Co, LTD, 2015. Feasibility Study Report on Project of Beijing Urban Rail Traffic Airport Line: Part of Ventilation and Air Conditioning, 9–10.

Beyler C L, Hirschler M. M., 1995. The SFPE handbook of fire protection engineering. Industrial safety & environmental protection.

Bilyaz, S., Buffington T., Ezekoye, O.A., 2021. The effect of fire location and the reverse stack on fire smoke transport in high-rise buildings. Fire. Safety. J. 126, 103446.

China Urban Railway Transit Association, 2023. Annual Statistics and Analysis Report on Urban Rail Traffic in 2022.

China Railway First Survey and Design Institude Group Co, LTD, 2013. Feasibility Study Report on Urumqi Urban Rail Traffic Line1 (SanTunBei-Airport): Part of Ventilation and Air Conditioning, 10–11.

Chen, J.F., Long, Z., Liu, C., Cai, S., Xu, B.Z., Cheng, H.H., 2022. Investigation of the performance of lateral ventilation in subway station fires. J. Wind. Eng. Ind. Aerod. 228, 105133.

Cheng, J.F., Zhong, M.H., Qiu, P.Y., Long, Z., Cheng, H.H., 2023. A study of repeatability of hot smoke test in a subway station. Case. Stud. Therm. Eng. 41,102666.

Cheng, X.D., Shi, Z.C., Nguyen K., Zhang L.H., Zhou Y., Zhang G.M., Wang J.H., Shi L., 2020. Solar chimney in tunnel considering energy-saving and fire safety. Energy, 210, 118601.

Chow, W.K., 1995. A comparison of the use of fire zone and field models for simulating atrium smoke-filling processes. Fire. Saf. J. 25, 337-53.

Domingo, J., Barbero, R., Iranzo, A., Cuadra, D., Servert, J., Marcos, M.A., 2011. Analysis and optimization of ventilation systems for an underground transport interchange building under regular and emergency scenarios. Tunn. Undergr. Space. Technol. 26, 179-188.

Dong, Y.H., Peng, F.L., Li, H., Men, Y.Q., 2023. Spatiotemporal characteristics of Chinese metro-led underground space development: A multiscale analysis driven by big data. Tunn. Undergr. Space. Technol. 139,105209.

Fan, C.G., Jin, Z.F., Zhang, J.Q., Zhu, H.Y., 2017. Effects of ambient wind on thermal smoke exhaust from a shaft in tunnels with natural ventilation. Appl. Therm. Eng. 117, 254-262.

Filis, V., Kolarik, J., Kevin Smith, M., 2021. The impact of wind pressure and stack effect on the performance of room ventilation units with heat recovery. Energ. Buildings. 234, 110689.

Gao, R., Li, A.G., Hao, X.P., Lei, W.J., Zhao, Y.J., Deng, B.S., 2012a. Fire-induced smoke control via hybrid ventilation in a huge transit terminal subway station. Energ. Buildings. 45, 280-289.

Gao, R., Li, A.G., Hao, X.P., Lei, W.J., Deng, B.S., 2012b. Prediction of the spread of smoke in a huge transit terminal subway station under six different fire scenarios. Tunn. Undergr. Space. Technol. 31,128-138.

Gao, R., Li, A.G., Zhang, Y., Luo, N., 2015. How domes improve fire safety in subway stations. Saf. Sci. 80, 94-104.

GB 51251, 2017. Technical Standard for Smoke Management Systems in Buildings. China Planning Press, Beijing.

Giachetti, B., Couton, D., Plourde, F., 2016. Smoke spreading analysis from an experimental subway scale model. Fire. Saf. J. 86, 75-82.

He, K., Shi, L., Zhang, S.G., Cong, W., Yang, H., Cheng, X.D., 2023. Experimental study on temperature attenuation of smoke flow driven by dual fire sources in a tunnel. Tunn. Undergr. Sp. Tech. 134, 105004.

Hu, M.Q., Liu, M., You, D., Zhang, Y.Z., 2020. Influence of train arrival characteristics on unorganized ventilation in underground subway station with platform screen doors. J. Wind. Eng. Ind. Aerod. 198, 104089.

Hu, L.H., Wu, L., Lu, K.H., Zhang, X.C., 2014. Optimization of emergency ventilation mode for a train on fire stopping beside platform of a metro station. Build. Simul-China. 7, 137-146.

Xie, M.X., Wang, J., 2023. Determination of pressure difference coefficient of shuttle elevator doors in super high-rise buildings under stack effect. Build. Environ. 232, 110076.

Ivanov, M.L., Peng, W., Wang, Q., Chow, W.K., 2021. Sustainable Smoke Extraction System for Atrium: A Numerical Study. Sustainability-Basel. 13, 7406.

Izadi, T., Mehrabian, M.A., Ahmadi, G., Abouali, O., 2021. Numerical analysis of the mirco-particles distribution inside an underground subway system due to train piston effect. J. Wind. Eng. Ind. Aerod. 211, 104533.

Jang Y.J., Kim, J.H., Rho, J.H., Yi, N.H., Hong, S.W., 2022. The characteristics of ventilated pool fires of Daegok-Sosa subway lines using Model-Scale tunnels and stations. Tunn. Undergr. Space. Technol. 121,104321.

Ji, J., Zhong, W., Li, K.Y., Shen, X.B., Zhang, Y., Huo, R., 2011. A simplified calculation method on maximum smoke temperature under the ceiling in subway station fires. Tunn. Undergr. Space. Technol. 26, 490-496.

Ji, J., Gao, Z.H., Fan, C.G., Sun, J.H., 2013. Large Eddy Simulation of stack effect on natural smoke exhausting effect in urban road tunnel fires. Int. J. Heat. Mass. Tran. 66, 531-542.

Ji, L.J., Si, Y.F., Liu, H.F., Song, X.L., Zhu, W., Zhu, A.P., 2014. Application of orthogonal experimental design in synthesis of mesoporous bioactive glass. Micropor. Mesopor. Mat. 184, 122-126.

Johansson N., Svensson, S., Heens, P.V., 2015. A study of reproducibility of a full-scale multi-room compartment fire experiment. Fire. Technol. 51, 645-665.

Klauck, M., Nobrega, G., Reinecke, E.A., Bentaib, A., Maas, L., Chaumeix, N., Allelein, H. J., 2022. Experimental investigation on the impact of cable fire products from flame-retardant cables on catalysts used in passive auto-catalytic recombiners. Prog. Nucl. Energ. 152, 104365.

Krol, M., Krol, A., 2017. Multi-criteria numerical analysis of factors influencing the efficiency of natural smoke venting of atria. J. Wind. Eng. Ind. Aerod. 170.,149-161.

Lan, B., Li, Y.R., Li, P.C., Gong, H.F., 2022. Numerical simulation of the chimney effect on smoke spread behavior in subway station fires. Case. Stud. Therm. Eng. 39, 102446.

Li, J., Yang, F.B., Zhang, H.G., Wu, Z., Tian Y.M., Hou X.C., Xu Y.H., Ren, J., 2020. Comparative analysis of different valve timing control methods for single-piston free piston expander-linear generator via an orthogonal experimental design. Energy, 195, 116966.

Li, Y.Z., Ingason, H., Liu, F., 2021b. Control of thermal-driven smoke flow at stairways in a subway platform fire. Int. J. Therm. Sci. 165, 106937

Li, J.X., Li, Y.F., Li, J.M., Li, X.J., Huang, Y.B., 2021a. Study on smoke control under mechanical exhaust strategy in a cross-type interchange subway station. Tunn. Undergr. Space. Technol. 112, 103897.

Lin, D., Nelson, J.D., Beecroft, M., Cui, J.Q., 2021. An overview of recent developments in China's

metro systems. Tunn. Undergr. Space. Technol. 111,103783.

Liu, C., Zhong, M.H., Tian, X.L., Zhang, P.H., Li, S.W., 2019. Study on emergency ventilation for train fire environment in metro interchange tunnel. Build. Environ. 147, 267-283.

Liu, F., Liu, Y.Q., Xiong, K., Weng, M.C., Wang, J., 2020. Experimental and numerical study on the smoke movement and smoke control strategy in a hub station fire. Tunn. Undergr. Space. Technol. 96, 103177.

Liu, Y.Q., Li Y.Z., Ingason, H., Liu, F., 2021. Control of thermal-driven smoke flow at stairways in a subway platform fire. Int. J. Therm. Sci. 165, 106937.

Liu, Y.Q., Liu, F., Weng, M.C., Obadi, I., Geng, P.Q., 2022. Research on thermal-driven smoke control by using smoke curtains during a subway platform fire. Int. J. Therm. Sci. 172, 107255.

Long, Z., Liu, C., Yang, Y.X., Qiu, P.Y., Tian, X.L., Zhong, M.H., 2020. Full-scale experimental study on fire-induced smoke movement and control in an underground double-island subway station. Tunn. Undergr. Space. Technol. 103, 103508.

Long, Z., Yang, Y.X., Liu, C., Zhong, M.H., 2021. Study on the optimal operation mode of ventilation system during metro double-island platform fire. Build. Simul-China. 14, 779–792.

Long, Z., Zhong, M.H., Chen, J.F., Cheng, H.H., 2023. Study on emergency ventilation strategies for various fire scenarios in a double-island subway station. 2023. J. Wind. Eng. Ind. Aerod. 235,105364.

Lu., X., Weng., M., Liu., F., Wang., F., Han., J., Chipok., C., 2022. Effect of bifurcation angle and fire location on smoke temperature profile in longitudinal ventilated bifurcated tunnel fires. Tunn. Undergr. Space Technol. 127, 104610.

Luo, N., Li, A.G., Gao, R., Song, T.Y., Zhang, W., Hu, Z.P., 2014. Performance of smoke elimination and confinement with modified hybrid ventilation for subway station. Tunn. Undergr. Space. Technol. 43,140-147.

Melcher T., Zinke, R., Trott, M., Krause, U., 2016. Experimental investigations on the repeatability of real scale fire tests. Fire. Saf. J. 82, 101-114.

McGrattan, K., Forney, G., 2018. Fire Dynamics Simulator (Version 6) User's Guide. Natl. Inst. Standards Technol.

Meng, N., Hu, L.H., Wu, L., Yang, L.Z., Zhu, S., Chen, L.F., Tang, W., 2014. Numerical study on the optimization of smoke ventilation mode at the conjunction area between tunnel track and platform in emergency of a train fire at subway station. Tunn. Undergr. Space. Technol. 40, 151-159.

Meng, N., Wang, Q., Liu, Z.X., Li, X., Yang, H., 2017. Study on the optimal operation mode of ventilation system during metro double-island platform fire tunnel ceiling for train fire at subway station: reduced-scale experiments and correlations. Appl. Therm. Eng. 115, 995–1003.

Oka, Y., Imazeki, O., 2014a. Temperature and velocity distributions of a ceiling jet along an inclined ceiling - Part 1: approximation with exponential function. Fire. Saf. J. 65, 41-52.

Oka, Y., Imazeki, O., 2014b. Temperature and velocity distributions of a ceiling jet along an inclined ceiling-Part 2: approximation based on cubic function and coordinate transformation. Fire. Saf. J. 65, 53-61.

Oka, Y., Imazeki, O., 2015. Temperature distribution within a ceiling jet propagating in an inclined flat-ceilinged tunnel with natural ventilation. Fire. Saf. J. 71, 20-33.

Pan, R.L., Zhu, G.Q., Xu, G., Liu, X., 2021. Experimental analysis on burning rate and temperature profile produced by pool fire in a curved tunnel as a function of fire location. Process. Saf. Environ. 152,549-567.

Park, W.H., Kim, D.H., Chang, H.C., 2006. Numerical predictions of smoke movement in a subway

station under ventilation, Tunn. Undergr. Space. Technol. 21, 304.

Peng, Y.Y., Gao, Z., W.W., Zhang, J.S., Li, X.Z., Xu, J.F., Wei, Y.L., 2021. Application of computational fluid dynamics in subway environment without fire and smoke—Literature review. Build. Environ. 206, 108408

Predvoditelev, A.S., Bubnov,V.A., 1972. Generalization of basic equations of aerodynamics and electrodynamics, Int. J. Heat. Mass. Tran. 15, 1185-1190.

Qi, D.H., Wang, L.Z., Zmeureanu, R., 2014, An analytical model of heat and mass transfer through non-adiabatic high-rise shafts during fires. Int. J. Heat. Mass. Tran. 72, 585-594.

Qin, T.X., Guo, Y.G., Lin, W.Y., 2009. Numerical simulation of the spread of smoke in an atrium under fire scenario. Build. Environ. 44, 56-65.

Rie, D.H., Hwang, M.W., Kim, S.J., Yoon, S.W., Ko, J.W., Kim, H.Y., 2006. A study of optimal vent mode for smoke control of subway station fire. Tunn. Undergr. Space. Technol. 21, 300-301.

Roh, J.S., Ryou, H.S., Park, W.H., Jang, Y.J., 2009. CFD simulation and assessment of life safety in a subway train fire. Tunn. Undergr. Space. Technol. 24, 447-453.

Shi, C.L., Li, J., Xu, X., 2021. Full-scale tests on smoke temperature distribution in long-large subway tunnels with longitudinal mechanical ventilation. Tunn. Undergr. Space. Technol. 109, 103784.

Tan, T.T., Yu, L.X., Ding, L., Gao, Z.H., Ji, J., 2021. Numerical investigation on the effect of ambient pressure on mechanical smoke extraction efficiency in tunnel fires. Fire. Safety. J. 120, 103136.

Tang, J.C., Gong, G.C., Su, H., Wu, F.H., Herman, C., 2016. Performance evaluation of a novel method of frost prevention and retardation for air source heat pumps using the orthogonal experiment design method. Appl. Energ. 169, 696-708.

Tian, X.L., Zhong, M.H., Shi, C.L., Zhang, P.H., Liu, C., 2017. Full-scale tunnel fire experimental study of fire-induced smoke temperature profiles with methanol-gasoline blends. Appl. Therm. Eng. 116,233-243.

Wang, k., Cai, W.Y., Zhang, Y.C., Hao, H.Q., Wang, Z.T.,2021. Numerical simulation of fire smoke control methods in subway stations and collaborative control system for emergency rescue. Process. Saf. Environ. 147,146-161.

Wang, W.H., He, T.F., Huang, W., Shen, R.Q., Wang, Q.S., 2018. Optimization of switch modes of fully enclosed platform screen doors during emergency platform fires in underground metro station. Tunn. Undergr. Space. Technol. 81, 277-288.

Wang, Y. f., Jiang J.C., Zhu D.Z.,2009. Full-scale experiment research and theoretical study for fires in tunnels with roof openings, Fire. Safety. J. 44, 339-348.

Wang, Z.L.; Zhu, L.; Guo, X.X.; Pan, X.H.; Zhou, B.; Yang, J.; Jiang, J.C.; Hua, M.; Feng, L.,2019. Reduced-scale experimental and numerical study of fire in a hybrid ventilation system in a large underground subway depot with superstructures under fire scenario. Tunn. Undergr. Space. Technol. 88, 98-112.

Xi, H., Zhang, H.H., He, Y.L., Zhuang, Z.H., 2019. Sensitivity analysis of operation parameters on the system performance of organic Rankine cycle system using orthogonal experiment. Energy. 172, 435-442.

Xu, D.S., Li, Y.F., Li, J.M., Zhang, J., 2021. Investigation on the effect of platform height on smoke characteristics of fire scenarios for subway stations. Sustainability-Basel. 13, 10584.

Xu, D.S., Li, Y.F., Li, J.X., Zhong, H., Li, J.M., Tu, D.K., Huang, Y.B., 2023. Evaluating the combustion and flame extension characteristics of cable fire in utility tunnels with spontaneous combustion scenarios: An experimental study. Tunn. Undergr. Space. Technol. 140, 105244.

Yamasawa, H., Kobayashi, T., Yamanaka, T., Choi, N., Cehlin, M., Ameen, A., 2021. Effect of supply velocity and heat generation density on cooling and ventilation effectiveness in room with impinging jet ventilation system. Build. Environ. 205, 108299.

Zhan, Q.S., Xiao, Y.Q., Zhang, L., Lin Z.H., Zou, Y.K., Liao, W., 2023. Hygrothermal performance optimization of lightweight steel-framed wall assemblies in hot–humid regions using orthogonal experimental design and a validated simulation model. Build. Environ. 236, 110262.

Zhang, C., Yang, J.S., Fu, J.Y., Wang, S.Y., Yin, J., Xie, Y.P., Li, L.Y., 2021. Cement based eco-grouting composite for pre-reinforcement of shallow underground excavation in vegetation protection area. Tunn. Undergr. Space. Technol. 118, 104188.

Zhang, L.M., Wu, X.G., Liu, M.J., Liu, W.L., Ashuri, B., 2019. Discovering worst fire scenarios in subway stations: a simulation approach. Autom. ConStruct. 99, 183-196.

Zhang, J., Li, Y.F., Dai, B.Q., Li, X.J., Huang, Y.B., 2018. The effect of exhaust velocity on smoke exhaust in subway platform fire. Procedia. Eng. 211, 1018-1025.

Zhang, S.G., Huang, Y.L., Shi, L., Lin, B., Li, X.B., Wu, Y.J., Wang, J.H., 2021. A fly-wing smoke screen to improve the smoke exhaustion performance of a vertical shaft in road tunnel. Tunn. Undergr. Space. Technol. 113,103983.

Zhao, D., Jiang, J.C., Zhou, R., Tong, Y., Wu, F., Shi, L.J., 2016. Numerical study on the optimisation of smoke ventilation mode for interchange subway station fire. Int. J. Vent. 15, 79-93.

Zhou, Y., Bu, R.W., Xu, Z.S., Chen, H.J., Gong, J.H., 2018. Numerical simulation of smoke control effectiveness with different exhaust modes in a large subway station. Procedia. Eng. 211, 1065-1074.

Zuo, W., E, J.Q., Liu, X.L., Peng, Q.G., Deng, Y.W., Zhu, H., 2016.Orthogonal Experimental Design and Fuzzy Grey Relational Analysis for emitter efficiency of the micro-cylindrical combustor with a step. Appl. Therm. Eng. 103, 945-951.